Russian Geology and Geophysics © 2019, V.S. Sobolev IGM, Siberian Branch of the RAS
Vol. 60, No. 10, pp. 1119–1140, 2019 *DOI:10.15372/RGG2019064* *Geologiya i Geofizika*

Mineralogy and Geochemistry of Ores of the Kedrovskoe–Irokinda Ore Field (Northern Transbaikalia)

O.Yu. Plotinskaya[a, ✉], A.V. Chugaev[a], D.B. Bondar[b], V.D. Abramova[a]

[a] *Institute of Geology of Ore Deposits, Petrography, Mineralogy and Geochemistry, Staromonetnyi per. 35, Moscow, 119017, Russia*

[b] *Bayerisches Geoinstitut, Universitätsstraße 30, University of Bayreuth, 95440 Bayreuth, Germany*

Received 6 March 2018; received in revised form 27 June 2018; accepted 26 July 2018

Abstract—Ore mineralogy of the Kedrovskoe–Irokinda ore field (northern Transbaikalia) has been studied. The ore field comprises ca. 200 quartz veins. Vein 3 and the Kvartsevaya and Serebryakovskaya veins of the Irokinda deposit and the Shamanovskaya, Pineginskaya, Osinovaya, and Barguzinskaya veins of the Kedrovskoe deposit have been described. Quartz–pyrite assemblage (quartz-1, pyrite, pyrrhotite, and marcasite) and quartz–gold–sulfide assemblage (quartz-2, galena, chalcopyrite, sphalerite, electrum, fahlore, Ag tellurides, and sulfosalts of Ag, Cu, Sb, Pb, and Sn) have been revealed. Major ore minerals were investigated by EPMA and LA-ICP-MS. An increase in Ag content in electrum (from 5.5 to 72.4 wt.%) and fahlores (from 5 to 35 wt.%) and in the abundance of Ag minerals during the ore formation has been established. Galena contains impurities of Sb and Ag (thousands of ppm), Se, Cd, Te, and Bi (hundreds of ppm), Cu, Zn, As, and Sn (tens of ppm). It is shown that the Kedrovskoe–Irokinda ore field is a rare type of orogenic deposits with considerable variations in the composition of major ore minerals (electrum, sphalerite, and fahlores), which is explained by the diversity of the host rocks.

Keywords: orogenic gold deposits, gold, sphalerite, galena, trace elements, LA-ICP-MS, Transbaikalia

INTRODUCTION

A significant amount of the world gold reserves is associated with orogenic deposits. Their genesis is one of the most debatable issues in modern ore geology (Buryak, 1982; Kerrich and Cassidy, 1994; Groves et al., 1998, 2003; Distler et al., 2004; Goldfarb and Groves, 2015). Such deposits are usually characterized by a high Au/Ag ratio (1–10) and a low variability of precious-metal minerals in ores, with a predominance of high-fineness native gold (Groves et al., 2003). However, there are deposits (e.g., Mother Lode (USA), Zun-Kholba (Russia), etc.) with a great diversity of Au and Ag minerals in ores, wide variations in native gold composition, and low Au/Ag ratios in ores (1:10 and less). These mineralogical and geochemical features and their reasons explain the interest of researchers to such deposits. The gold deposits of the Kedrovskoe–Irokinda ore field (KIOF) also belong to this type. They were classified as orogenic based on the structural control of mineralization (manifested as large vein zones) and on the absence of lateral geochemical zonation and genetic relationship with intrusions (Goldfarb et al., 2014; Chugaev et al., 2017; Bondar' et al., 2018).

The Kedrovskoe–Irokinda ore field, located on the slopes of the South Muya ridge (Muya district, Republic of Buryatia), has been studied for more than 50 years (Bazhenov et al., 1970; Mitrofanov et al., 1970; Lyakhov and Popivnyak, 1977). Mineral composition of certain ore zones (Khrustalev and Khrustaleva, 2006; Bondar' et al., 2018), geologic structure (Zlobina et al., 2014; Popov et al., 2017a), wallrock alteration (Kucherenko, 2004, 2006a,b, 2014; Popov et al., 2017b), and sources of ore matter (Chugaev et al., 2017) have been described.

The factors that determined the mineral and geochemical compositions of the KIOF gold mineralization have not been considered yet. This made it necessary to study the chemical composition of Au- and Ag-minerals and associated major ore minerals by electron probe microanalysis (EPMA) and laser ablation inductively coupled plasma mass spectrometry (LA-ICP-MS).

BRIEF GEOLOGY OF THE KEDROVSKOE–IROKINDA ORE FIELD

The Kedrovskoe–Irokinda ore field, which comprises the Kedrovskoe gold deposit (~28 tons Au (Zapadnaya..., 2018)), the Irokinda gold deposit (~24 tons Au (Norgold, 2018), and a number of ore occurrences, is situated in the north of the Transbaikalian folded region. The ore field is confined to the Muya segment of the Baikal–Muya Orogenic Belt (BMOB), one of major structural units of the Central Asian Orogenic Belt (Zhmodik et al., 2006; Rytsk et al., 2011; Yarmolyuk et al., 2012) (Fig. 1*a*).

✉ Corresponding author.
E-mail adress: plotin-olga@ya.ru (O.Yu. Plotinskaya)

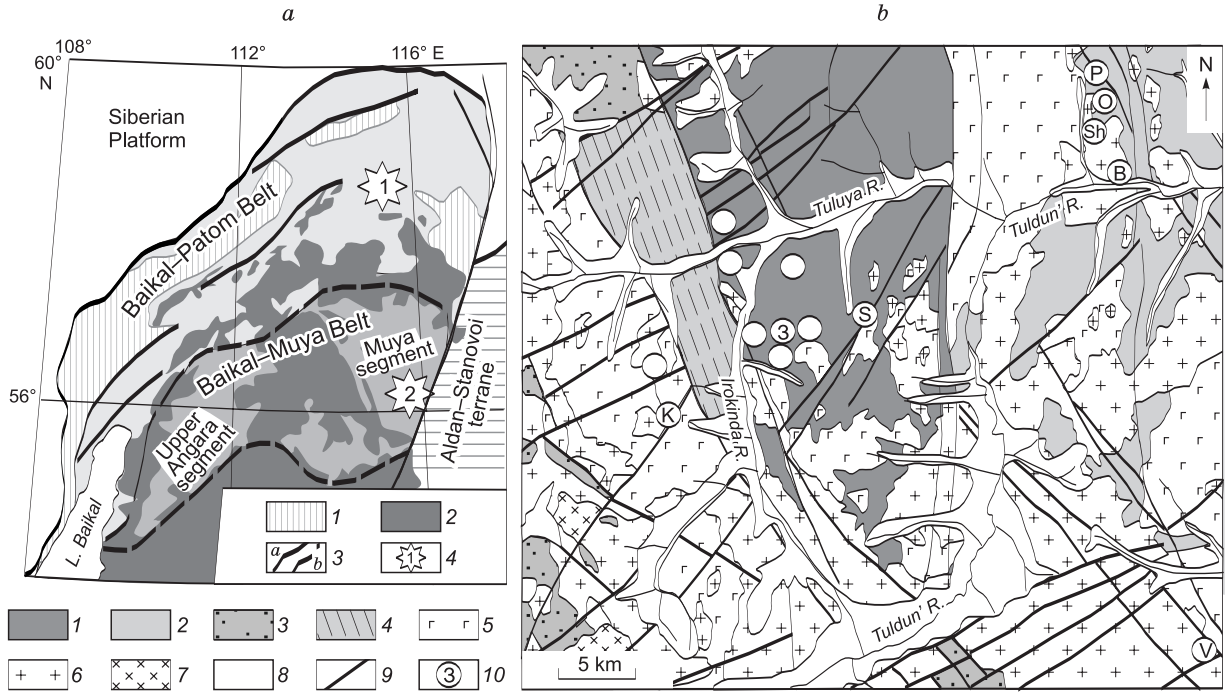

Fig. 1. *a*, Tectonic scheme of the Baikal–Vitim terrane in the northern part of the Transbaikalian folded region, modified after Gusev and Khain (1995) and Rytsk et al. (2001). *1*, uplifts of the early Proterozoic basement in the Baikal–Patom belt; *2*, Paleozoic granitoids (Angara–Vitim batholith); *3*, regional faults: *a*, thrusts and shifts, *b*, suture zones; *4*, gold deposits: 1, Sukhoi Log; 2, Kedrovskoe–Irokinda ore field. *b*, Schematic geologic structure of the Kedrovskoe–Irokinda ore field (northern Transbaikalia), after Zapadnaya Gold Mining Ltd. *1*, gneiss, schist, marble, and calciphyre of the Kindikan Formation (AR); *2*, metasedimentary rocks (metasandstone, biotite binary mica schist, sericite–chlorite schist, limestone, and carbonaceous shale) of the Parama Group (PR_2); *3*, orthoschist, mica–quartz schist, metaeffusive rocks, and tuff conglomerates of the Ust'-Kelyana Formation (PR_2); *4*, molassoid (conglomerate, gravelstone, sandstone, and schist) sediments of the Amatkan Formation (PR_3); *5*, gabbroid of the Kedrovsky complex (PR_2); *6*, granitoid of the Bambukoi complex (PR_2); *7*, granitoid of the Vitimkan complex (PZ_2); *8*, alluvial sediments (Q); *9*, major faults; *10*, ore zones: Irokinda deposit: K, Kvartsevaya, 3, Vein 3, S, Serebryakovskaya; Kedrovskoe deposit: B, Barguzinskaya; Sh, Shamanovskaya; O, Osinovaya; P, Pineginskaya; V, Vitimkon ore occurrence.

Precambrian rocks dominate within the KIOF (State..., 2010) (Fig. 1*b*). The metamorphic rocks of the Kindikan Formation (para- and orthogneisses, schists, marbles, and calciphyres) are the oldest; they compose an uplift of the Archean basement (South Muya block). Some researchers, however, regard these rocks as Proterozoic (Skuzovatov et al., 2016).

The Neoproterozoic stratified rocks include terrigenous-carbonate units of the Kedrovskoe and Ust'-Tuldun' Formations of the Parama Group, volcanosedimentary rocks of the Ust'-Kelyana Formation (U–Pb (ID TIMS) zircon age is 824 ± 2 Ma (Rytsk et al., 2001)), and late Ediacaran molassoid sediments of the Amatkan Formation. The rocks underwent regional greenschist facies and contact metamorphism.

The Kedrovsky and Bambukoi igneous complexes of the KIOF are Neoproterozoic intrusions. The Kedrovsky igneous complex has a Sm–Nd age of 735 ± 26 Ma (Rytsk et al., 2001) and includes zonal massifs composed of gabbro, gabbronorites, anorthosites, and their transitional varieties (Tsygankov et al., 1998). The Bambukoi complex is formed by granitoid intrusions (leucogranites, biotite and biotite–amphibole granites, and granodiorites) localized mainly along the periphery of the South Muya block. The U–Pb (ID TIMS) age of granites is 723 ± 4 Ma (Rytsk et al., 2001).

Paleozoic igneous rocks are scarce in the KIOF. These are compositionally diverse dike complexes (dolerites, lamprophyres, diorites, and granite porphyry) and small granitoid massifs of the Vitimkan (or Konkuder–Mamakan) complex dated at 292 ± 1 Ma (State..., 2010; Tsygankov et al., 2010). They formed as a result of the Hercynian global transformation of the BMOB continental crust and the formation of the large (more than 150,000 km^2) multiphase Angara–Vitim batholith (Tsygankov et al., 2010).

The main structural units of the KIOF are the above-mentioned uplift of the crystalline basement, the Kelyana–Irokinda suture zone bounding the South Muya block from the southeast, and a system of deep faults of NE (Ozernoe-Serebryakovo zone) and E–W (Kindikan and Tuluin zones) strikes, which determined the block structure of the ore field (from the unpublished report by Yu.V. Pivovarov et al. (Oktyabr'skaya Geological Exploration Party) in 1975).

Within the KIOF, gold mineralization is localized in quartz veins hosted by Precambrian rocks of different compositions and origin. The geologic structures control the localization of orebodies. The veins are spatially confined to regional tectonic zones of the KIOF and are conformable with them in dip and strike. There are about 200 gold-bear-

ing quartz veins 0.3 to 3 m (on average, ~1 m) in thickness. Their length varies from 60 to 1500 m along the strike and from 100 to 400 m in dip. The veins are accompanied by quartz–sericite alteration aureoles up to 20 m in thickness (Mitrofanov et al., 1970; Kucherenko, 2004, 2014; Khrustalev and Khrustaleva, 2006).

The Irokinda deposit is located in the southwest of the KIOF, on the western periphery of the South Muya block. Most of ore veins are hosted by Archean gneisses and schists of the Kindikan Formation. The Kelyana–Irokinda suture zone and fissure faults are the principal ore-controlling structures. About 10 ore zones (veins) have been explored within the deposit. At present, Vein 3 and the Vysokaya, Serebryakovskaya, and Kvartsevaya veins are exploited.

The Kedrovskoe deposit is located east of the South Muya block. Orebodies are localized within terrigenous metasedimentary rocks of the Kedrovskoe Formation and within Neoproterozoic gabbroids and granitoids of the Kedrovsky pluton. Gold mineralization is confined to faults of the Tuldun' tectonic zone. Five ore zones have been explored in detail and are currently exploited: Osinovaya, Shturmovaya, Shamanovskaya, Pineginskaya, and Yuzhnaya.

The Vitimkon ore occurrence is located southeast of the Irokinda deposit. Gold-bearing quartz veins occur in the zone of contact between granitoids of the Bambukoi complex and gabbroids of the Kedrovsky complex.

Gold mineralization formed in the KIOF at 280–270 Ma (early Permian), during the final phases of late Paleozoic regional magmatism (Kucherenko, 1989, 2006a,b; Chugaev et al., 2017).

Several veins have been studied: Vein 3, Kvartsevaya, and Serebryakovskaya at the Irokinda deposit and Shamanovskaya, Pineginskaya, Osinovaya-1, and Barguzinskaya at the Kedrovskoe deposit (Table 1).

MAJOR MINERAL ASSEMBLAGES AND MINERAL FORMATION SEQUENCE

All KIOF veins have a similar mineral composition. The major gangue mineral is quartz (up to 99%); nests of muscovite and carbonates of the dolomite–ankerite series are often present. Massive or coarse-clastic quartz is predominant. It is often foliate as a result of multiple shifts parallel

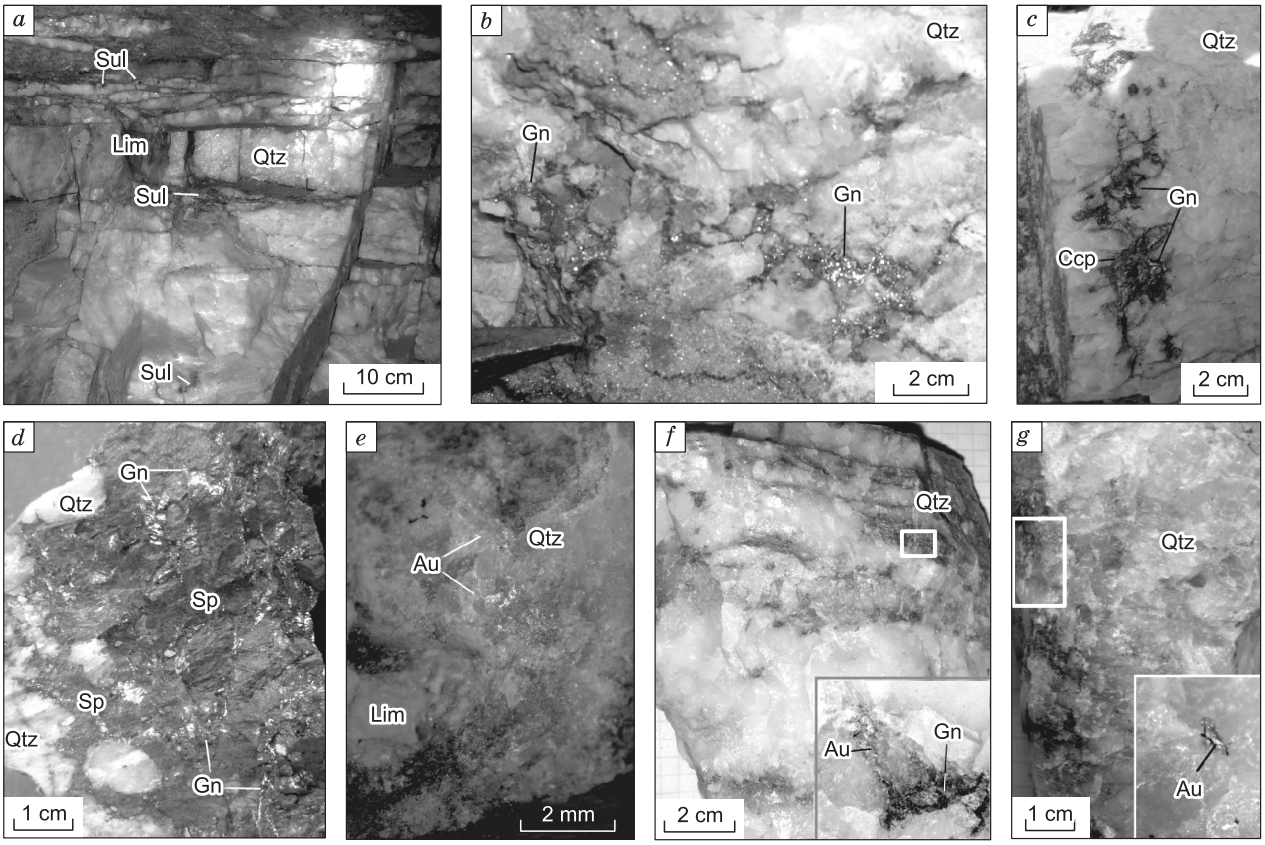

Fig. 2. Relationships among ore and gangue minerals in the Irokinda (*a*, *b*, *f*, *g*) and Kedrovskoe (*c*, *d*) deposits. *a*, Massive pseudofoliated quartz (Qtz) with sulfide nests (Sul) and minor limonite (Lim), Vein 3; *b*, nest-like galena dissemination (Gn) in quartz, Serebryakovskaya vein; *c*, galena and chalcopyrite (Ccp) in quartz, Pineginskaya vein, sample K-26/15; *d*, large sphalerite nest (Sph) with galena containing quartz relics, Pineginskaya vein, sample K-13/15; *e*–*g*, visible gold (Au): *e*, Vitimkon ore occurrence, sample Vit-1; *f*, Serebryakovskaya vein, sample Ir-87/13; *g*, Kvartsevaya vein, sample Ir-69/13.

Table 1. Characteristics of the studied KIOF ore samples

Sample	Sampling location	Characteristics
Irokinda deposit		
Ir-6/13	*Vein 3*, adit 49, level 1090 m, mark 29	Quartz vein in gneiss of the Kindikan Formation. Coarse-clastic quartz with large galena nests
Ir-15/13	*Vein 3*, adit 49, level 1040 m, mark 76	Quartz vein in crystalline rocks of the Kindikan Formation. White, locally translucent, quartz. Nests of sulfides (galena crystals (up to 1 cm in size), brown sphalerite (up to 0.5 cm), and scarce pyrite metacrysts (up to 2–3 cm))
Ir-16/13	*Vein 3*, adit 49, level 1040 m, mark 76	Quartz vein in crystalline rocks of the Kindikan Formation. White quartz, translucent near sulfides. Nests of sulfides (galena, brown sphalerite, and scarce pyrite metacrysts up to 2–3 cm in size)
Ir-18/13	*Vein 3*, adit 49, level 1040 m, mark 68	Quartz vein with sulfide mineralization in crystalline rocks of the Kindikan Formation
Ir-20/13	*Vein 3*, adit 49, level 1040 m, mark 68	Quartz vein in crystalline rocks of the Kindikan Formation. White quartz brecciated by a dense network of galena stringers merging into nests up to 2 cm in size, with 0.5 cm and larger galena crystals and pyrite dissemination
Ir-64/13	*Kvartsevaya vein*, dumps of adit 61	White ferruginous quartz with sulfide (galena + chalcopyrite) nests up to 0.5 cm in size and an elongate 2 × 2 × 0.5 cm nest
Ir-69/13	*Kvartsevaya vein*, dumps of adit 61	Quartz vein ~10 cm thick. Nests of pyrite (up to 1 cm), chalcopyrite, galena, and native gold (Fig. 2*g*)
Ir-80/13	*Serebryakovskaya vein*, adit 78, level 1120 m, raise 1	Quartz vein with large galena grains in crystalline rocks of the Kindikan Formation
Ir-87/13	*Serebryakovskaya vein*, dumps of adit 12	Quartz vein in crystalline rocks of the Kindikan Formation. White pseudofoliated quartz (the strips are gray because of disseminated galena) with impurities of native gold (Fig. 2*f*)
Kedrovskoe deposit		
K-1A-5	*Osinovaya vein*, adit 17, raise 26, level 1000 m	Quartz vein with a pyrite nest 2–3 cm in size and disseminated galena
K-3-3	*Osinovaya vein*, adit 25, raise 15 bis, level 960.4 m	Quartz vein with galena and pyrite nests up to 1 cm in size
K-4-4	*Osinovaya vein*, sublevel 26 m, level 921.4 m	Galena, sphalerite, and pyrite nests in vein quartz
K-7-5	*Osinovaya vein*, adit 16, block 25, level 814 m	Pyrite and galena nests and scarce sphalerite dissemination in vein quartz
K-8-2	*Osinovaya vein*, block 23, sublevel 63/1 m, level 786.9 m	Quartz vein with a large galena nest
K-9-5	*Osinovaya vein*, Severnyi BIS gallery, level 755.3 m	Nest of massive, partly pyritized pyrrhotite with galena stringers and sphalerite nests
K-12/14	*Osinovaya vein*, adit 25, level 950 m, mark 45	Quartz vein with sulfide mineralization (pyrite, galena, and sphalerite) in granodiorites of the Bambukoi complex
K-12a/14	*Osinovaya vein*, sublevel 920 m	Quartz vein with sulfide mineralization (pyrite, galena, and sphalerite) in granodiorites of the Bambukoi complex
K-16/14	*Osinovaya vein*, adit 16, Yuzhnyi BIS gallery, level 810 m	Quartz vein with sulfides, with pyrite and galena at the contact with carbonaceous–micaceous silty shales
K-13/15	*Osinovaya ore zone, Promezhutochnaya vein*, adit 25, raise 48	Large (>10 cm) sphalerite nest with numerous galena veinlets and fragments of white quartz (Fig. 2*c*)
K-19/14	*Shamanovskaya vein*, surficial sampling. 56°2′45.33″ N, 115°33’4.53″ E	Quartz vein with sulfides, with pyrite and galena at the contact with carbonaceous–micaceous silty shales
K-26/15	*Pineginskaya vein*, adit 26, level 925 m	Quartz vein with chalcopyrite and galena (Fig. 2*c*)
B-1/15	*Barguzinskaya vein*, adit 10, level 460, slope 5, adit end	Quartz vein with sulfide mineralization (pyrite, pyrrhotite, sphalerite, and galena) in granodiorites
Vit-1	*Vitimkon ore occurrence,* surficial sampling, 55°50′ 19.98″N, 115°33′ 47.89″E	Quartz vein with numerous limonite and scarce native gold (Fig. 2*e*)

to selvages (Fig. 2*a*) (data by Yu.V. Pivovarov et al., 1975). Kucherenko (2014) notes the presence of dolerite dikes cutting quartz veins and crossed by quartz veinlets bearing ore mineralization.

Ore minerals are extremely unevenly distributed in the veins. They occur as fine dissemination and small nests varying in size from few millimeters to tens of centimeters (Fig. 2*b–d*). The total amount of ore minerals usually does not exceed 1%, except for the Osinovaya vein (Kedrovskoe deposit), where it reaches 5%. Major ore minerals are pyrite, galena, and sphalerite, whereas pyrrhotite, chalcopyrite, fahlores, scheelite, and native gold are much scarcer. Native gold is sometimes present as grains up to 1–2 mm in size and is seen with the naked eye (Fig. 2*e–g*).

The KIOF shows no noticeable changes in structural plan or intersection of veins. This indicates that there was only one ore (productive) stage within the KIOF. The intersection of minerals in thin sections permitted us to recognize quartz–pyrite and quartz–gold–polysulfide assemblages (substages) (Fig. 3).

At the **quartz–pyrite** substage, quartz veins and quartz-sericite wallrock alteration with pyrite dissemination and most of pyrite in veins formed. Pyrrhotite-1, which forms massive bodies or large nests in the lower horizons of the Osinovaya and Barguzinskaya veins, seems to have been produced at the same substage. Pyrrhotite-1 is often replaced by marcasite-1 (specific "bird's eye" textures), which is then replaced by pyrite (Fig. 4*b*, *c*). It cannot be ruled out that early high-fineness gold considered below is also part of this mineral assemblage.

Quartz–gold–polysulfide (or gold–sphalerite–galena) assemblage formed later than the quartz veins and is accompanied by "new" quartz (often translucent), "pseudofoliated" quartz at the vein selvages, and, sometimes, carbonates (e.g., dolomite–ankerite in the Serebryakovskaya vein). Galena is the most abundant ore mineral, and chalcopyrite, sphalerite, native gold, and fahlore are somewhat scarcer. The minerals of this assemblage form nests in vein quartz or fill cracks and veinlets in pyrite (Fig. 4*c*, *d*). Galena and fahlore often overgrow and cement earlier chalcopyrite and sphalerite (Fig. 4*e*). Sometimes this assemblage includes pyrrhotite-2, which, together with galena and chalcopyrite, forms veins in pyrite and which is almost completely replaced by marcasite-2 (Fig. 4*f*).

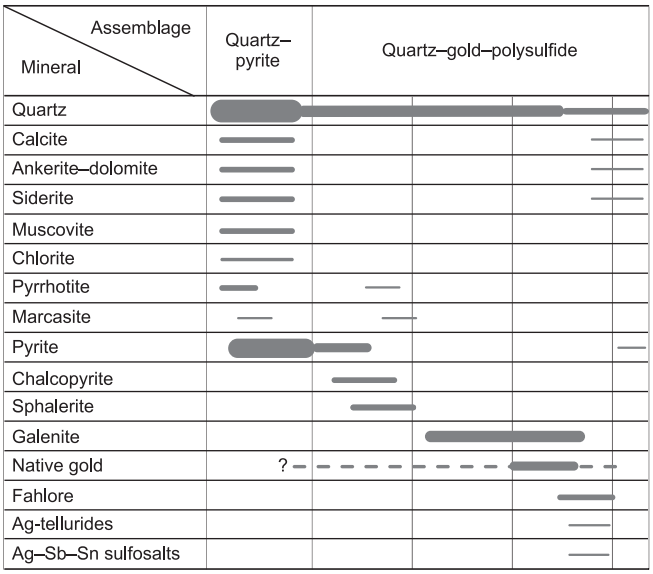

Fig. 3. Schematic sequence of hypogene mineral formation in the KIOF. Compiled after Mitrofanov et al. (1970), Lyakhov and Popivnyak (1977), Khrustalev and Khrustaleva (2006), and Bondar' et al. (2018).

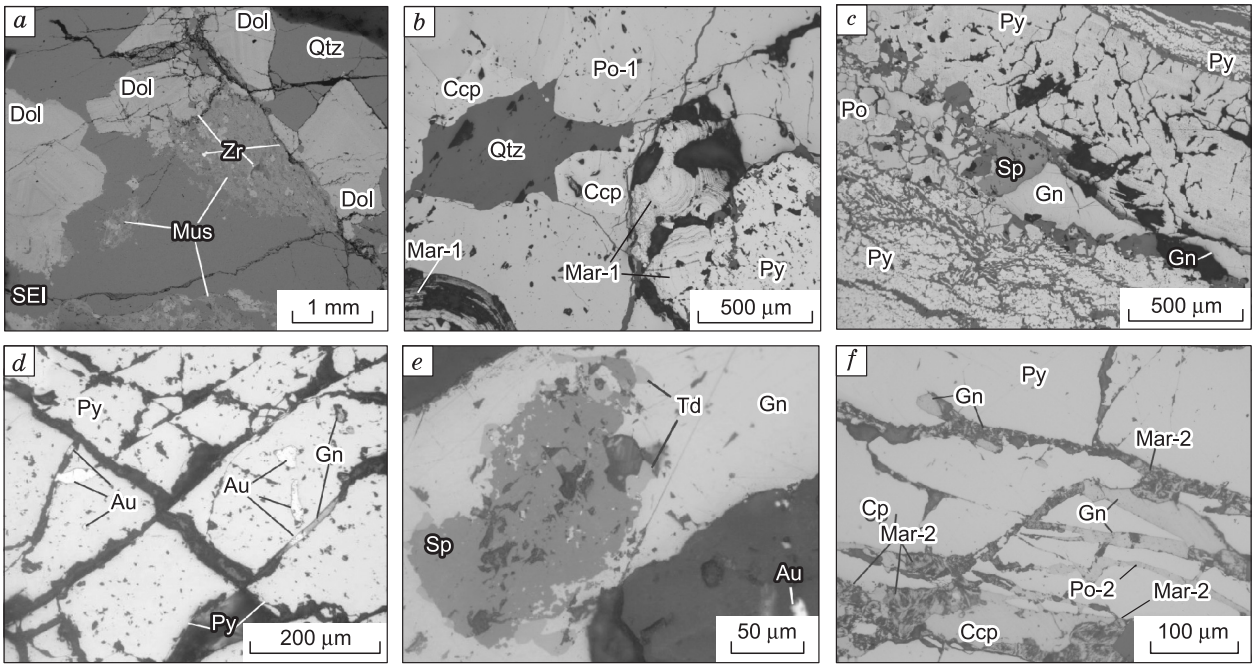

Fig. 4. Relationships among ore and gangue minerals in the Kedrovskoe (*a*–*c*, *f*) and Irokinda (*d*, *e*) deposits. *a*, Dolomite crystals (Dol) and muscovite nests (Mus) with zircon dissemination (Zr) in quartz (Qtz), Shamanovskaya vein, sample K-19/14; *b*, pyrrhotite-1 (Po-1) is replaced by marcasite-1 (Mar-1), which is replaced by pyrite (Py), and chalcopyrite (Ccp) is localized along the boundary between pyrrhotite-1 and quartz, Barguzinskaya vein, sample V-1/15; *c*, galena veinlet (Gn) with sphalerite (Sp) crosses an aggregate of pyrrhotite-1 almost completely replaced by pyrite, Osnovnaya vein, sample K-9-5; *d*, native gold (Au) and galena form veinlets in pyrite, Vein 3, sample Ir-20/13; *e*, galena overgrows sphalerite, with fahlore (tetradymite (Td)) developed at their contact, quartz contains native gold, Vein 3, sample Ir-6/13; *f*, galena, chalcopyrite, pyrrhotite-2, and marcasite-2 form veinlets in pyrite, Osinovaya vein, sample K-4-4.

METHODS

Mineral composition was studied with electron microscopes equipped with energy-dispersive detectors: Tescan Vega TS 5130 MM (CamScan) with an INCA Energy 350 detector and an INCA Penta FETx3 detector, Tescan Vega II XMU with an INCA Energy 450 detector and an INCA xSight detector (Institute of Experimental Mineralogy, Chernogolovka, analyst A.N. Nekrasov), and JEOL JSM-6480LV with an INCA X-MaxN-50 detector (Department of Petrology, Moscow State University, analyst N.N. Koshlyakova).

The main ore minerals were analyzed on a JXA-8200 (JEOL, Japan) microprobe at the IGEM-Analitika Shared Facilities Center, Moscow (analysts I.G. Griboedova, E.V. Koval'chuk, S.E. Borisovskii, and V.I. Taskaev). Operation conditions: accelerating voltage 20 kV, sample current 20 nA, and beam diameter 1 μm.

Native gold. Analytical lines: L_α—Au and Ag, K_α—Cu, and M_β—Hg. Standards: chemically pure metals for Au and Ag and HgS for Hg. Exposition time: Au and Ag—10 s at the peak and 5 s on the background on either side of it, Cu and Hg—20 s at the peak and 10 s on the background on either side of it; detection limits—0.04–0.08 wt.%.

Fahlores. Analytical lines and standards: Sb (L_α)—Sb_2S_3, Se (L_α)—CdSe, Zn (K_α)—ZnS, S (K_α)—$CuFeS_2$, Ag (L_α)—$AgSbS_2$, As (L_α)—GaAs, Cu (K_α)—Cu, Hg (M_α)—HgS, Te (L_α)—Te, Fe (K_α)—$CuFeS_2$, Bi (M_α)—Bi_2Te_3, Cd (L_β)—CdSe, and Pb (M_α)—PbS. Exposition time: 10 s at the peak and 5 s on the background on either side of it. Detection limits (2σ) (wt.%): S—0.01, Se and Fe—0.04, Ag—0.05, As, Cu, Te, and Pb—0.05, Hg and Bi—0.06, Sb and Zn—0.07, and Cd—0.10.

Sphalerite. Analytical lines: K_α—S, Zn, Fe, Mn, and Cu, L_α—Cd and Sn, and M_α—Hg. Standards: ZnS for S and Zn, $CuFeS_2$ for Fe, HgS for Hg, and chemically pure metals for Mn, Sn, and Cu. Exposition time (peak/background): S and Zn—10/5 s, Fe, Hg, Mn, Sn, and Cu—20/10 s, and Cd—30/15 s. Detection limits: 0.02–0.06 wt.%.

Galena. Analytical lines and standards: Sb (L_α)—Sb_2S_3, Se (L_α)—CdSe, S (K_α)—ZnS, Ag (L_α)—$AgSbS_2$, As (L_α)—GaAs, Cu (K_α)—Cu, Fe (K_α)—$CuFeS_2$, Bi (M_α)—Bi_2Te_3, Cd (L_β)—CdSe, Pb (M_α)—PbS, and Bi (M_α) Bi. Exposition time (peak/background): S, Pb, Se, and Ag—10/5 s, Cu—20/5 s, Fe, Sb, and As—20/10 s, and Bi—30/15 s. Detection limits: 0.02–0.06 wt.%.

The composition of galena was studied by LA–ICP-MS on a Thermo Xseries quadrupole mass spectrometer with a New Wave 213 laser ablation system at the IGEM-Analitika Shared Facilities Center of the Institute of Geology of Ore Deposits, Petrography, Mineralogy and Geochemistry, Moscow. The following isotopes were measured: S^{33}, V^{51}, Cr^{53}, Mn^{55}, Fe^{57}, Co^{59}, Ni^{60}, Cu^{65}, Zn^{66}, Ga^{69}, Ge^{72},As^{75}, Se^{77}, Mo^{95}, Ag^{107}, Cd^{111}, In^{115}, Sn^{118}, Sb^{121},Te^{125}, W^{182}, Au^{197}, Hg^{202}, Tl^{205}, Pb^{207}, and Bi^{209}, which were chosen because of the minimum isobaric and molecular interferences. Isotope Pb^{207} was used instead of more common Pb^{208} to reduce the stress on the detector. In addition, a qualitative analysis for isotopes Si^{29}, Ca^{44}, and Ti^{47} was made to exclude possible inclusions of silicates, carbonates, and Ti minerals in galena. The analysis was carried as linear profiles no longer than 1 mm; operating conditions: ablation speed 5 μm/s, spot size 80 μm, laser frequency 15 Hz, and input power 5–7 J/cm^2. The evaporated sample substance was supplied with a helium flow (600 ml/min) into the plasma of the mass spectrometer ion source. The background signal was measured for 30 s before each analysis; the washout time after each analysis was 30 s. Data were collected using the time-resolved mode. The integration time for each mass was 10 ms. The drift of the instrumental parameters was corrected using S^{33} as an internal standard in accordance with the stoichiometric composition of galena (13.4 wt.%). The MASS1C (US Geological Survey) was used as an external standard. The data were processed using the Iolite software (Paton et al., 2011). Detection limits (ppm): V—0.2, Cr—0.8, Mn—0.5, Fe—14, Co—0.04, Ni—0.6, Cu—0.8, Zn—2, Ga—0.02, Ge—0.3, As—0.9, Se—4, Mo—0.06, Ag—0.03, Cd—0.6, In—0.03, Sn—0.1, Sb—0.2, Te—1, W—0.03, Au—0.07, Hg—0.2, Tl—0.004, Pb − 6, and Bi—0.02.

CHEMICAL COMPOSITION OF MAJOR ORE MINERALS

Galena. Galena is the most common ore mineral after pyrite in the Kedrovskoe–Irokinda ore field. It forms large nests younger than the vein quartz groundmass (Fig. 2*b*, *c*). This determines the angular morphology of most of galena grains. Galena overgrows pyrite and sphalerite and fills pores and cracks in these minerals. It is often saturated with numerous oval or rounded inclusions of other minerals (Figs. 5 and 6), usually sulfosalts or tellurides. Tetrahedrite is the most common sulfosalt in galena of Vein 3 of the *Irokinda* deposit (Fig. 5*a*–*c*). Sometimes it occurs as uniformly disseminated isometric grains 10–30 μm in size (Fig. 5*b*). Ulmanite NiSbS (Ni = 25.9–27.4, Sb = 55.9–58.1, and S = 14.6–15.3 wt.%, according to nine analyses) was found in Vein 3 and the Serebryakovskaya vein (Fig. 5*d*). Occasional grains of bournonite $CuSbS_2$ (Cu = 12.1, Pb = 42.8, Sb = 25.1, and S = 20.0 wt.%, one analysis) were identified only in Vein 3 (Fig. 5*b*).

Galena of the Kvartsevaya vein contains acicular segregations of tetradymite Bi_2Te_2S (Bi = 57.2, Te = 36.7, and S = 4.3 wt.%, one analysis) (Fig. 5*e*). Inclusions of Ag tellurides are often found in Vein 3 and the Serebryakovskaya vein (Fig. 5*c*, *f*, *g*). Hessite Ag_2Te is the commonest mineral (Table 2, ans. 1–4); stützite $Ag_{5-x}Te_3$ (Table 2, an. 5) and empressite AgTe (Fig. 5*f*, *g*, Table 2, an. 6) are much scarcer. Sometimes they are intergrown with partly decomposed native tellurium (Fig. 5*f*).

In galena of the Shamanovskaya vein in the *Kedrovskoe* deposit, we have found elongate or oval inclusions of poly-

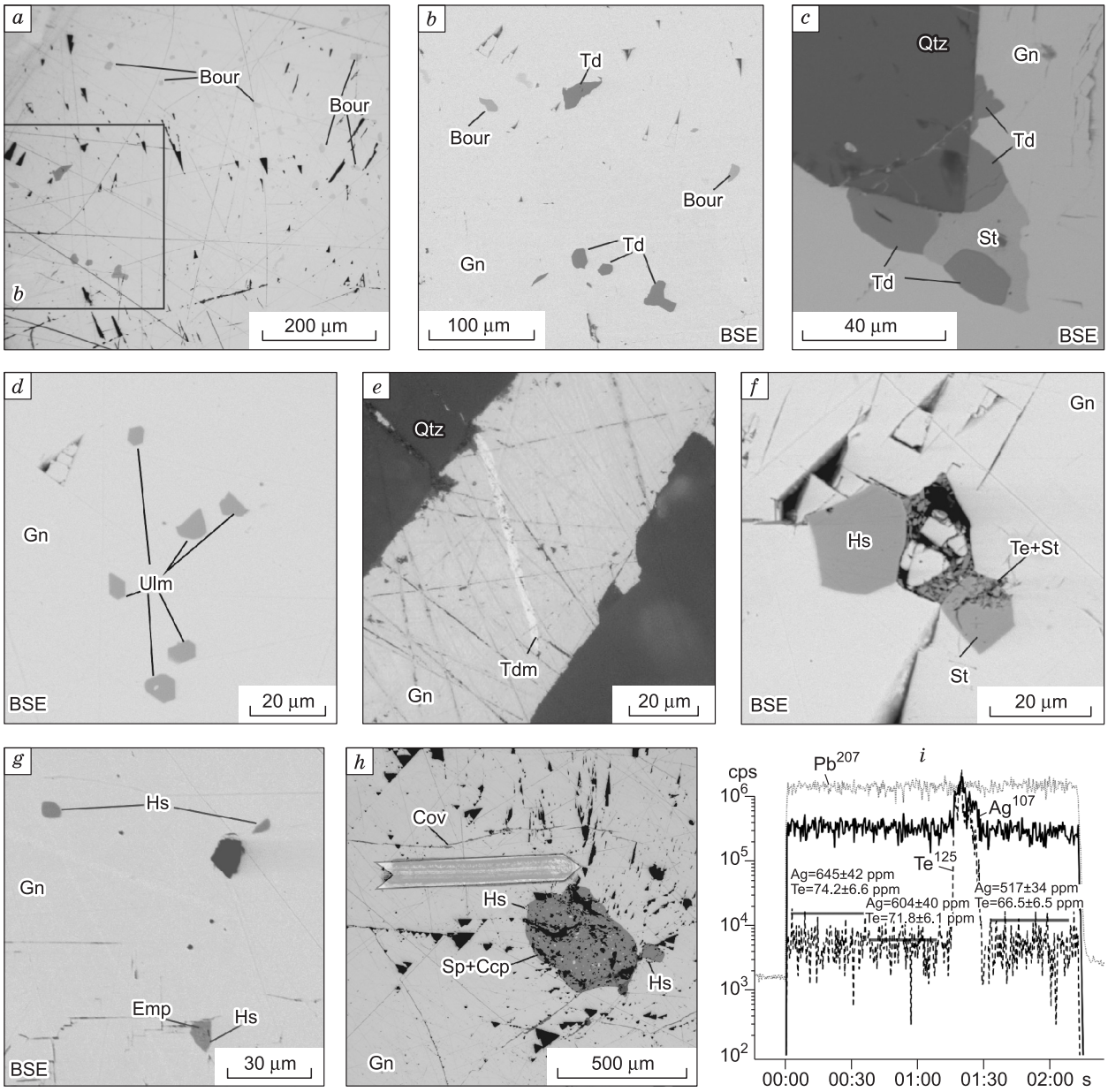

Fig. 5. Mineral inclusions in galena from the Irokinda deposit. *a–d*, Vein 3: *a*, numerous inclusions of bournonite (Bour) and tetrahedrite (Td) in galena, sample Ir-6/13, *b*, magnified fragment of *a*, *c*, stützite (St) and tetrahedrite at the galena (Gn)/quartz (Qtz) boundary, sample Ir-6/13; *d*, ulmanite (Ulm) inclusions in galena (Gn), sample Ir-16/13; *e*, Kvartsevaya vein, sample Ir-69/13, tetradymite (Tdm) in galena; *f–g*, Serebryakovskaya vein, sample Ir-80/13; *f*, hessite (Hs), stützite (St), and native tellurium relics (Te) in galena; *g*, hessite (Hs) and empressite (Emp) in galena; *h*, galena with sphalerite and hessite inclusions; *i*, variations in the intensities of Ag^{107}, Te^{125}, and Pb^{207} along the ablation line profile and contents of Ag and Te in the calculation intervals. Hereafter, BSE, back-scattered electron images.

basite $Cu(Ag,Cu)_6Ag_9Sb_2S_{11}$ few tens to few hundreds of microns in size (Fig. 6*a*, Table 2, ans. 9–15). Polybasite is often intergrown with diaphorite $Ag_3Pb_2Sb_3S_8$ (Ag = 25.0–27.6, Cu = 0.2–0.9, Sb = 23.2–27.4, Pb = 25.9–32.2, and S = 17.9–19.4 wt.%, seven analyses) and canfieldite Ag_8SnS_6 grains (Table 2, ans. 21–23) no larger than few tens of microns.

In the *Osinovaya* vein, we have found hessite (Fig. 6*b*, *d*, *e*, Table 2, ans. 7 and 8), tetrahedrite (*c*, *d*), canfieldite (Fig. 6*d*, *f*), and a phase similar in composition to polybasite (Fig. 6*e*, *f*; Table 2). The latter differs from polybasite in lower contents of Cu (Table 2, ans. 16–20). Polybasite of similar composition was earlier revealed in the Jáchymov ore district, Czech Republic (Ondruš et al., 2003). The KIOF polybasite and canfieldite always have significant contents of Te (9.8–19.2 and 15.7–16.8 wt.%, respectively), which isomorphically substitutes sulfur (Bindi et al., 2012, 2013).

Table 2. Chemical composition of mineral inclusions in galena from the Irokinda (1–6) and Kedrovskoe (7–29) deposits, wt.% (results of energy-dispersive analysis)

No.	Sample	S	Cu	Ag	Sb	Sn	Te	Total	Formula
1	Ir-20/13	–	–	62.19	–	–	37.65	99.84	$Ag_{1.98}Te_{1.02}$
2	Ir-20/13	–	–	62.85	–	–	38.35	101.20	$Ag_{1.98}Te_{1.02}$
3	Ir-80/13	–	–	62.91	–	–	35.59	98.50	$Ag_{2.03}Te_{0.97}$
4	Ir-80/13	–	–	63.71	–	–	36.49	100.20	$Ag_{2.02}Te_{0.98}$
5	Ir-80/13	–	–	58.27	–	–	40.25	98.52	$Ag_{5.05}Te_{2.95}$
6	Ir-80/13	–	–	43.69	–	–	53.71	97.39	$Ag_{0.98}Te_{1.02}$
7	K-8-3	–	–	62.81	–	–	35.38	98.19	$Ag_{2.03}Te_{0.97}$
8	K-7-5	–	–	63.98	–	–	36.70	100.68	$Ag_{2.02}Te_{0.98}$
9	K-19/14	10.73	1.82	64.76	9.20	–	12.45	98.96	$(Ag_{15.31}Cu_{0.73})_{16.04}Sb_{1.93}(S_{8.54}Te_{2.49})_{11.03}$
10	K-19/14	11.63	2.12	66.51	8.99	–	9.78	99.03	$(Ag_{15.37}Cu_{0.83})_{16.20}Sb_{1.84}(S_{9.04}Te_{1.91})_{10.95}$
11	K-19/14	10.16	1.45	64.69	9.22	–	13.94	99.46	$(Ag_{15.47}Cu_{0.59})_{16.06}Sb_{1.95}(S_{8.17}Te_{2.82})_{10.99}$
12	K-19/14	11.74	2.87	68.64	8.04	–	8.06	99.35	$(Ag_{15.68}Cu_{1.11})_{16.79}Sb_{1.63}(S_{9.02}Te_{1.56})_{10.58}$
13	K-19/14	10.60	1.45	64.29	9.08	–	13.53	98.95	$(Ag_{15.29}Cu_{0.59})_{15.88}Sb_{1.91}(S_{8.49}Te_{2.72})_{11.21}$
14	K-19/14	9.90	1.16	64.20	8.53	–	13.72	97.51	$(Ag_{15.69}Cu_{0.48})_{16.17}Sb_{1.85}(S_{8.14}Te_{2.84})_{10.98}$
15	K-19/14	10.27	1.35	64.57	8.19	–	13.54	97.92	$(Ag_{15.59}Cu_{0.55})_{16.14}Sb_{1.75}(S_{8.34}Te_{2.76})_{11.10}$
16	K-8-2	8.69	0.35	64.32	8.24	–	18.21	99.81	$(Ag_{15.96}Cu_{0.15})_{16.11}Sb_{1.81}(S_{7.26}Te_{3.82})_{11.08}$
17	K-8-2	8.88	0.41	64.94	8.38	–	18.68	101.29	$(Ag_{15.87}Cu_{0.17})_{16.04}Sb_{1.82}(S_{7.29}Te_{3.86})_{11.15}$
18	K-8-2	9.43	0.35	65.79	8.75	–	15.93	100.25	$(Ag_{15.99}Cu_{0.15})_{16.14}Sb_{1.89}(S_{7.71}Te_{3.27})_{10.98}$
19	K-8-2	9.57	0.25	65.62	8.82	–	15.87	100.13	$(Ag_{15.93}Cu_{0.10})_{16.03}Sb_{1.90}(S_{7.82}Te_{3.26})_{11.08}$
20	K-7-5	8.94	0.67	64.48	8.13	–	18.78	101.00	$(Ag_{15.74}Cu_{0.28})_{16.02}Sb_{1.76}(S_{7.34}Te_{3.88})_{11.22}$
21	K-19/14	10.15	–	63.39	–	7.89	16.07	97.49	$Ag_{8.04}Sn_{0.91}(S_{4.33}Te_{1.72})_{6.05}$
22	K-19/14	9.90	–	65.90	–	8.24	15.08	99.12	$Ag_{8.28}Sn_{0.94}(S_{4.18}Te_{1.60})_{5.78}$
23	K-19/14	10.40	–	63.67	–	7.12	16.84	98.02	$Ag_{8.00}Sn_{0.81}(S_{4.40}Te_{1.79})_{6.19}$
24	K-8-2	10.30	–	64.05	–	7.67	17.33	99.36	$Ag_{7.98}Sn_{0.87}(S_{4.32}Te_{1.83})_{6.15}$
25	K-8-2	9.91	–	65.36	–	7.86	17.67	100.80	$Ag_{8.12}Sn_{0.89}(S_{4.14}Te_{1.86})_{6.00}$
26	K-8-2	9.44	–	65.16	–	6.53	18.43	99.55	$Ag_{8.25}Sn_{0.75}(S_{4.02}Te_{1.97})_{5.99}$
27	K-8-2	10.16	–	65.47	–	7.77	17.62	101.02	$Ag_{8.08}Sn_{0.87}(S_{4.22}Te_{1.84})_{6.06}$
28	K-8-2	10.24	–	65.69	–	7.70	16.64	100.27	$Ag_{8.13}Sn_{0.87}(S_{4.26}Te_{1.74})_{6.00}$
29	K-8-2	10.24	–	66.33	–	7.86	17.04	101.47	$Ag_{8.13}Sn_{0.88}(S_{4.22}Te_{1.77})_{5.99}$

Note. 1–4, 7, 8, hessite; 5, stützite; 6, empressite; 9–20, polybasite; 21–29, canfieldite.

The morphology and distribution of mineral inclusions within the galena grains suggest that they formed either simultaneously with the deposition of the host mineral or somewhat later, as, for example, tetrahedrite, which grows over galena or replaces it in cracks and pores.

A probe microanalysis of galena showed that the contents of most of trace elements (Ag, Sb, Bi, Cd, As, Cu, Fe, and Se) are below their detection limits. The exceptions are the samples Ir-69/13 (Bi = 0.35–0.65 wt.%, Ag ≤ 0.07 wt.%, and Se ≤0.17 wt.%, 11 analyses), K-19/14 (Sb = 0.08–0.20 wt.% and Ag = 0.10–0.23 wt.%, four analyses), K-4-4 (Sb ≤ 0.11 wt.% and Ag ≤0.09 wt.%, six analyses), and K-8-2 (Sb ≤ 0.08 wt.% and Ag = 0.07–0.14 wt.%, three analyses).

For LA–ICP-MS analysis of trace elements in galena, we chose grain sites free of mineral inclusions. For this reason, the sample Ir-6/13 was not studied (Fig. 5*a*). Nevertheless, the examined profiles had intervals similar in composition to the mineral inclusions in galena. For example, the sample Ir-80/13 (Serebryakovskaya vein, Irokinda deposit) shows synchronous peaks of Ag^{107} and Te^{125}, apparently corresponding to hessite inclusions (Fig. 5*h*, *i*), and the sample K-19/14 shows peaks of Te^{125} and Au^{197}. These intervals were excluded from the data processing and calculation of trace-element contents in galena. In the other cases, almost all trace elements demonstrate rather uniform LA-ICP-MS profiles corresponding to the uniform distribution of trace elements in galena.

The main trace elements in the KIOF galena (Table 3) are Sb (up to 0.5 wt.%) and Ag (up to 0.25 wt.%). The contents of Se, Cd, Te, and Bi reach a few hundred ppm (except for the sample Ir-69/13 containing 0.35 wt.% Bi), and the contents of Cu, Zn, As, and Sn, up to several tens of ppm. The content of Tl permanently present in galena usually does not exceed 0.5 ppm. Approximately a half of the samples have

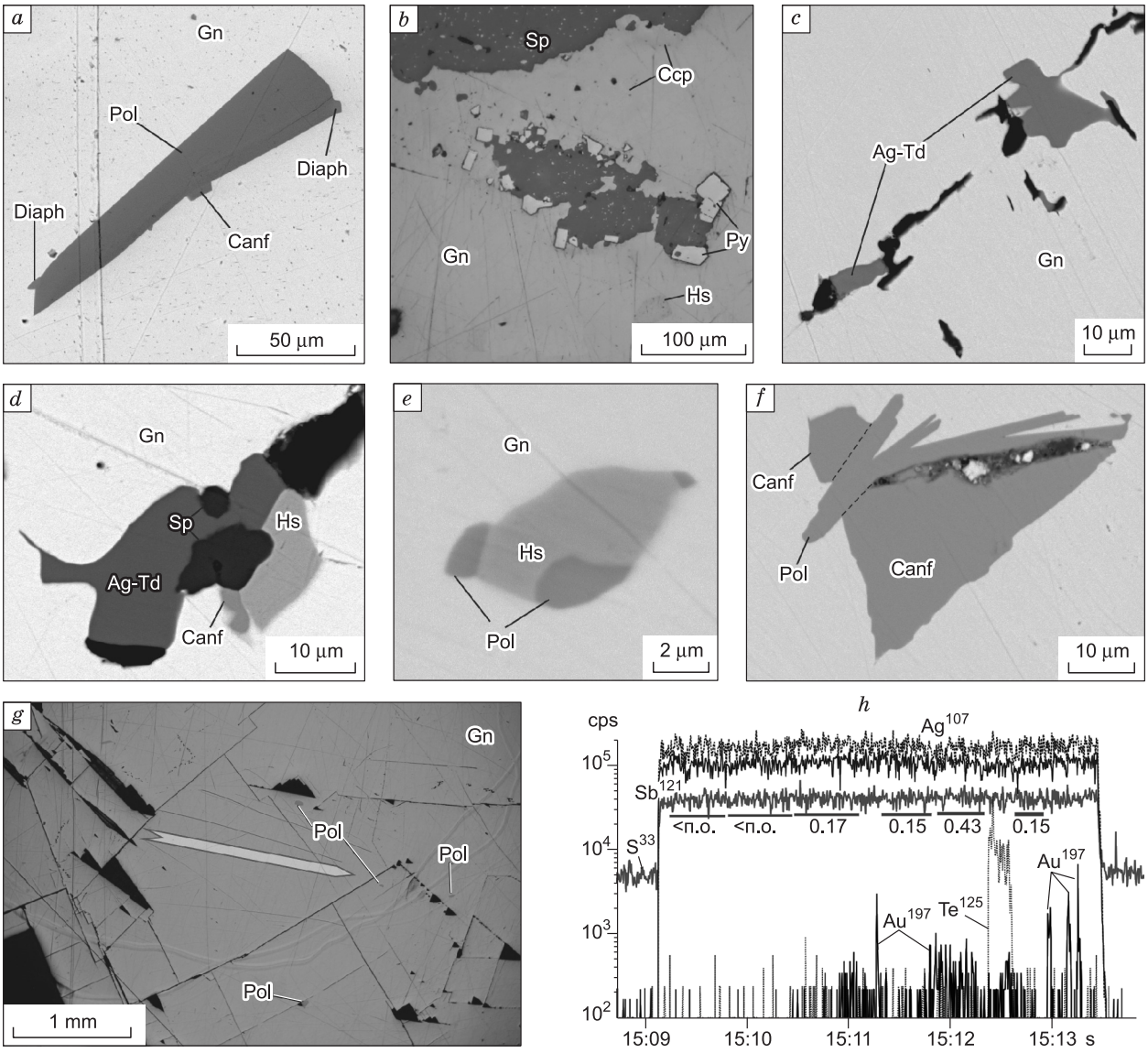

Fig. 6. Mineral inclusions in galena from the Kedrovskoe deposit, Shamanovskaya (*a*) and Osinovaya vein (*b–g*) veins. *a*, Polybasite (Pol), canfieldite (Canf), and diaphorite (Diaph), sample K-19/14; *b*, hessite, sphalerite, pyrite, and chalcopyrite, sample K-7-5; *c*, chain of tetrahedrite grains (Ag-Td), sample K-8-2; *d,* tetrahedrite, hessite, canfieldite, and sphalerite, sample K-7-5; *e*, hessite and polybasite, sample K-8-2; *f*, canfieldite and polybasite, sample K-8-2; *g*, galena with inclusions of Ag sulfosalts, sample K-19/14; *h*, variations in the intensities of S^{33}, Ag^{107}, Sb^{121}, Te^{125}, and Au^{197} along the ablation profile and contents of Au in the calculation intervals.

contents of In above its detection limit but mostly no higher than 0.1 ppm. The contents of Au above its detection limit, 0.5 ppm, are found only in the samples K-19/14 and Ir-80/13. The contents of V, Mn, Fe, Hg, Co, Ni, Ga, Ge, W, and Mo are below their detection limits in all of the studied samples. The content of Sb in the Kedrovskoe deposit is, in general, higher than that in the Irokinda deposit (Fig. 7); in both deposits it varies considerably from sample to sample (Table 3, Appendix A (http://sibran.ru/journals/Appendix A_27-06-18.xlsx)). The contents of Ag, As, Zn, Cu, and Tl in the Kedrovskoe and Irokinda deposits are rather similar (Fig. 7, Table 3). The contents of Cd and Sn in the Kedrovskoe deposit (about 150 and 10 ppm, respectively) are, on the average, an order of magnitude higher than those in the Irokinda deposit, but the contents of Bi, Se, and Te are, on the contrary, lower.

Fahlores. Minerals of this group are scarce in the KIOF. In addition to the above-mentioned fine inclusions in galena, they occur as intergrowths with galena and, more seldom, pyrite, sphalerite, and other minerals. Their grains are seldom larger than few hundred microns (Fig. 8*a*, *b*). In chemical composition all studied fahlores correspond to tetrahedrite with domination of Fe over Zn and with high contents of Ag.

In **the Irokinda deposit** (*Vein 3*), fahlores are intimately intergrown with galena, which suggests their nearly simultaneous formation (Fig. 8*a*). They are chemically homoge-

Table 3. Summary of trace-element contents in galena (ppm) from the Kedrovskoe and Irokinda deposits (LA-ICP-MS data)

Deposit, vein, sample	Sample	Cu	Zn	As	Se	Ag	Cd	In	Sn	Sb	Te	Tl	Bi
Kedrovskoe, Osinovaya, K-1A-5	Geom. mean (5)	4.9	2.1	51	192	496	108	—	2.4	963	13	0.07	30
	S.d.	1.3	0.39	1.7	11	112	14	—	1.0	210	2.0	0.01	1.2
	Min	3.6	1.8	49	179	348	92	<D.l.	1.2	714	11	0.06	29
	Max	6.4	2.8	53	205	623	129	0.04	3.7	1217	17	0.08	32
Kedrovskoe, Osinovaya, K-3-3	Geom. mean (5)	2.1	2.3	45	62	403	138	0.11	18	856	78	0.28	2.4
	S.d.	0.28	0.40	3.9	12	24	6.1	0.03	2.2	49	6.0	0.04	0.08
	Min	2.0	1.9	39	51	374	130	0.08	16	793	71	0.22	2.3
	Max	2.6	2.9	49	77	431	146	0.16	20	906	85	0.32	2.5
Kedrovskoe, Osinovaya, K-4-4	Geom. mean (8)	1.0	5.2	37	29	775	225	—	15	1675	55	0.12	1.1
	S.d.	0.21	5.1	7.9	2.5	32	13	—	1.7	128	12	0.02	0.06
	Min	0.74	1.9	25	25	736	196	<D.l.	14	1480	38	0.11	1.0
	Max	1.3	16	47	33	815	236	0.06	18	1890	72	0.15	1.1
Kedrovskoe, Osinovaya, K-7-5	Geom. mean (7)	1.8	4.2	51	151	735	105	0.05	11	1472	39	0.33	26
	S.d.	0.20	2.1	2.3	9.0	246	51	0.02	5.4	493	4.8	0.03	0.75
	Min	1.6	2.7	48	140	534	69	0.03	6.4	1062	33	0.29	25
	Max	2.0	9.0	53	164	1068	178	0.08	19	2100	45	0.38	27
Kedrovskoe, Osinovaya, K8-2	Geom. mean (8)	1.6	3.6	55	41	935	212	—	1.1	1999	11	0.23	7.4
	S.d.	0.24	0.51	3.8	7.0	31	11	—	0.27	51	2.4	0.01	0.62
	Min	1.2	2.9	50	33	898	195	<D.l.	0.81	1939	7.4	0.20	6.5
	Max	1.9	4.3	59	48	1004	230	0.05	1.6	2087	15	0.25	8.6
Kedrovskoe, Osinovaya, K-13/15	Geom. mean (9)	—	1.9	18	32	659	107	0.06	6.9	905	41	0.13	36
	S.d.	—	0.46	2.4	2.2	21	9.1	0.01	0.19	61	6.5	0.01	1.5
	Min	<D.l.	1.4	15	29	624	93	0.04	6.7	834	35	0.11	34
	Max	<D.l.	2.7	22	36	688	116	0.08	7.2	994	53	0.15	38
Kedrovskoe, Shamanovskaya, K-19/14	Geom. mean (11)	31	2.2	56	359	2194	289	0.06	1.1	4511	2.7	0.14	121
	S.d.	4.5	0.63	1.9	13	194	25	0.01	0.14	371	0.86	0.01	4.9
	Min	23	0.90	53	336	1910	259	0.05	0.88	3970	1.8	0.12	114
	Max	38	3.1	60	378	2510	324	0.08	1.3	5040	4.2	0.16	129
Irokinda, Vein 3, Ir-16/13	Geom. mean (4)	3.1	2.1	48	210	665	9.7	0.02	0.65	1277	25	0.27	128
	S.d.	0.64	0.32	3.3	7.8	24	0.38	0.01	0.09	55	1.1	0.01	4.7
	Min	2.8	1.7	46	204	641	9.2	0.02	0.54	1219	25	0.26	123
	Max	4.1	2.4	53	220	699	10	0.03	0.74	1351	27	0.29	133
Irokinda, Vein 3, Ir-20/13	Geom. mean (6)	4.2	1.9	50	191	649	8.3	—	0.35	1297	22	0.27	87
	S.d.	0.95	0.74	2.1	6.8	33	0.48	—	0.10	97	1.0	0.01	4.2
	Min	3.3	1.2	48	180	585	7.5	<D.l.	0.26	1109	21	0.25	81
	Max	5.7	3.4	53	198	675	8.8	<D.l.	0.54	1371	24	0.28	93
Irokinda, Kvartsevaya, Ir-69/13	Geom. mean (5)	47	—	29	447	1869	38	—	—	60	552	0.26	3381
	S.d.	4.4	—	2.3	108	174	7.1	—	—	6.0	82	0.03	78
	Min	43	<D.l.	26	374	1714	32	<D.l.	<D.l.	53	456	0.22	3280
	Max	53	<D.l.	31	617	2160	50	<D.l.	<D.l.	69	668	0.29	3480
Irokinda, Serebryakovskaya, Ir-80/13	Geom. mean (6)	3.8	5.2	49	317	574	42	0.05	1.4	1169	69	0.35	57
	S.d.	14	0.79	2.9	19	46	3.4	0.01	0.09	110	4.2	0.06	2.0
	Min	1.5	4.4	46	280	517	38	0.05	1.2	1047	63	0.30	55
	Max	37	6.6	53	334	645	46	0.08	1.5	1351	74	0.43	60

Note. Parenthesized is the number of analyses; S.d., standard deviation; <D.l., below the detection limit.

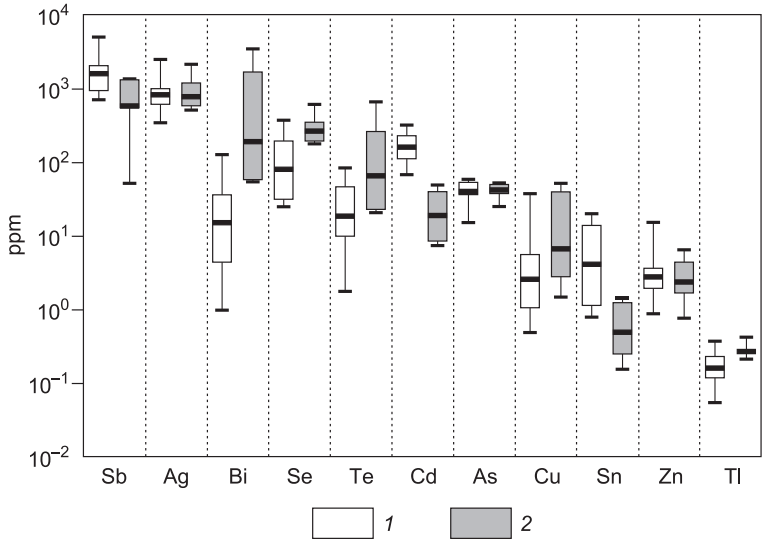

Fig. 7. Box and whisker plots for major trace elements in galena of the Kedrovskoe and Irokinda deposits. Box covers the interval with 25–75% of all values; whisker shows the whole range. Black horizontal line marks the geometric mean. Deposits: *1*, Kedrovskoe, *2*, Irokinda.

neous; the contents of Ag vary from 10.9 to 16.7 wt.% (Table 4, ans. 1–11).

In *the Pineginskaya vein* of **the Kedrovskoe deposit** (sample K-26/15), fahlores with Ag ~ 25 wt.% are intimately intergrown with galena (Table 4, ans. 12–13). The intergrowths are rimmed by later formed fahlore (Fig. 8*b*) of inhomogeneous structure (Fig. 8*c*) with Ag = 31.6–33.8 wt.% (Table 4, ans. 14–15). Fahlores present as inclusions in galena from *the Osinovaya vein* are similar in composition to fahlores of the Pineginskaya vein but show a somewhat

Table 4. Chemical composition of fahlores from the Irokinda (1–11) and Kedrovskoe (12–22) deposits, wt.% (electron probe microanalysis data)

No.	Sample	Note	Cu	Ag	Fe	Zn	Cd	Pb	Sb	As	Bi	S	Se	Total	Formula
1	Ir-6/13	Intimate intergrowth with galena (Fig. 8*a*)	27.08	14.49	4.41	1.72	<D.l.	0.15	27.21	0.17	0.08	23.30	<D.l.	98.61	$(Cu_{7.6}Ag_{2.4})_{10.0}(Fe_{1.4}Zn_{0.5})_{1.9}(Sb_{4.0}As_{0.0})_{4.0}S_{13.0}$
2			28.23	13.36	4.47	1.97	<D.l.	0.14	27.58	0.14	0.03	23.49	<D.l.	99.39	$(Cu_{7.9}Ag_{2.2})_{10.1}(Fe_{1.4}Zn_{0.6})_{2.0}(Sb_{4.0}As_{0.0})_{4.0}S_{13.0}$
3			29.20	13.09	4.34	2.10	<D.l.	0.09	26.63	0.58	<D.l.	23.56	0.03	99.61	$(Cu_{8.1}Ag_{2.1})_{10.2}(Fe_{1.4}Zn_{0.5})_{1.9}(Sb_{3.84}As_{0.14})_{4.0}S_{12.9}$
4			30.37	10.86	4.40	2.22	<D.l.	0.15	26.82	0.49	0.10	23.58	<D.l.	99.00	$(Cu_{8.4}Ag_{1.7})_{10.1}(Fe_{1.4}Zn_{0.6})_{2.0}(Sb_{3.9}As_{0.1})_{4.0}S_{12.9}$
5			28.37	13.32	4.16	2.20	<D.l.	0.18	27.09	0.26	<D.l.	23.41	<D.l.	99.00	$(Cu_{7.9}Ag_{2.2})_{10.1}(Fe_{1.3}Zn_{0.6})_{1.9}(Sb_{3.9}As_{0.1})_{4.0}S_{12.95}$
6		Inclusions	27.43	13.78	4.79	1.14	0.37	0.20	27.24	0.14	0.04	23.31	0.04	98.49	$(Cu_{7.7}Ag_{2.3})_{10.0}(Fe_{1.5}Zn_{0.3}Cd_{0.1})_{1.9}Sb_{4.0}S_{13.0}$
7			27.69	13.53	4.56	1.37	0.29	0.12	27.46	0.13	0.05	23.48	0.05	98.71	$(Cu_{7.8}Ag_{2.2})_{10.0}(Fe_{1.4}Zn_{0.4}Cd_{0.1})_{1.9}Sb_{4.0}S_{13.0}$
8			27.44	13.18	4.38	1.97	0.02	0.21	27.61	0.19	0.05	22.93	<D.l.	97.97	$(Cu_{7.8}Ag_{2.2})_{10.0}(Fe_{1.4}Zn_{0.6})_{2.0}Sb_{4.1}S_{12.9}$
9*			25.03	16.56	5.10	<D.l.	<D.l.	<D.l.	28.67	<D.l.	<D.l.	24.64	<D.l.	100.00	$(Cu_{7.1}Ag_{2.7})_{9.8}Fe_{1.6}Sb_{4.2}S_{13.3}$
10*			25.56	16.12	4.73	0.64	<D.l.	<D.l.	28.61	<D.l.	<D.l.	24.34	<D.l.	100.00	$(Cu_{7.3}Ag_{2.6})_{9.9}(Fe_{1.5}Zn_{0.2})_{1.7}Sb_{4.2}S_{13.2}$
11*			25.77	15.13	4.87	0.82	<D.l.	<D.l.	28.75	<D.l.	<D.l.	24.67	<D.l.	100.00	$(Cu_{7.3}Ag_{2.4})_{9.7}(Fe_{1.6}Zn_{0.2})_{1.8}Sb_{4.2}S_{13.3}$
12	K-26/15	Core (Fig. 8*b*, *c*)	20.34	25.28	3.11	3.33	0.28	0.05	25.55	0.14	0.06	22.87	<D.l.	100.99	$(Cu_{5.8}Ag_{4.3})_{10.1}(Fe_{1.0}Zn_{0.9}Cd_{0.1})_{2.0}Sb_{3.9}S_{13.0}$
13			20.80	25.02	2.98	3.44	0.17	0.12	25.68	0.10	0.08	22.73	<D.l.	101.12	$(Cu_{6.0}Ag_{4.2})_{10.2}(Fe_{1.0}Zn_{1.0})_{2.0}(Sb_{3.9})_{3.9}S_{12.94}$
14		Rim (Fig. 8*b*, *c*)	13.82	33.84	5.52	0.55	<D.l.	0.10	25.04	0.00	0.14	20.70	0.07	99.77	$(Cu_{4.2}Ag_{6.1})_{10.3}(Fe_{1.9}Zn_{0.2})_{2.1}Sb_{4.0}S_{12.6}$
15			16.09	31.56	4.66	1.75	<D.l.	0.04	25.52	0.03	<D.l.	21.32	0.06	101.04	$(Cu_{4.8}Ag_{5.5})_{10.3}(Fe_{1.6}Zn_{0.5})_{2.1}Sb_{4.0}S_{12.6}$
16*	K-7-5	Owergrows galena	22.66	22.19	5.56	0.23	<D.l.	<D.l.	27.94	<D.l.	<D.l.	23.93	<D.l.	102.51	$(Cu_{6.3}Ag_{3.6})_{9.9}(Fe_{1.8}Zn_{0.1})_{1.9}Sb_{4.0}S_{13.2}$
17*			23.14	21.19	5.51	0.36	<D.l.	<D.l.	28.03	<D.l.	<D.l.	24.08	<D.l.	102.32	$(Cu_{6.4}Ag_{3.5})_{9.9}(Fe_{1.7}Zn_{0.1})_{1.8}Sb_{4.1}S_{13.2}$
18*		Fig. 6*d*	23.34	20.15	3.09	3.13	<D.l.	<D.l.	28.36	<D.l.	<D.l.	24.43	<D.l.	102.50	$(Cu_{6.5}Ag_{3.3})_{9.8}(Fe_{1.0}Zn_{0.8})_{1.8}Sb_{4.1}S_{13.4}$
19*	K-8-2	Fig. 6*c*	13.63	34.56	4.74	0.46	<D.l.	<D.l.	26.18	<D.l.	<D.l.	21.16	<D.l.	100.73	$(Cu_{4.1}Ag_{6.2})_{10.3}(Fe_{1.6}Zn_{0.2})_{1.8}Sb_{4.1}S_{12.7}$
20*			13.36	35.03	4.67	0.33	<D.l.	<D.l.	25.89	<D.l.	<D.l.	21.06	<D.l.	100.34	$(Cu_{4.1}Ag_{6.3})_{10.4}(Fe_{1.6}Zn_{0.1})_{1.7}Sb_{4.1}S_{12.7}$
21*			13.37	34.19	3.90	0.17	<D.l.	<D.l.	25.50	<D.l.	<D.l.	20.84	<D.l.	97.96	$(Cu_{4.2}Ag_{6.3})_{10.5}(Fe_{1.4}Zn_{0.1})_{1.5}Sb_{4.1}S_{12.9}$
22*	K-8-3	In galena	13.39	32.40	4.96	0.36	<D.l.	<D.l.	24.68	<D.l.	<D.l.	21.99	<D.l.	97.78	$(Cu_{4.1}Ag_{5.8})_{9.9}(Fe_{1.7}Zn_{0.1})_{1.8}Sb_{3.9}S_{13.3}$

* Energy-dispersive analysis. <D.l., below the detection limit.

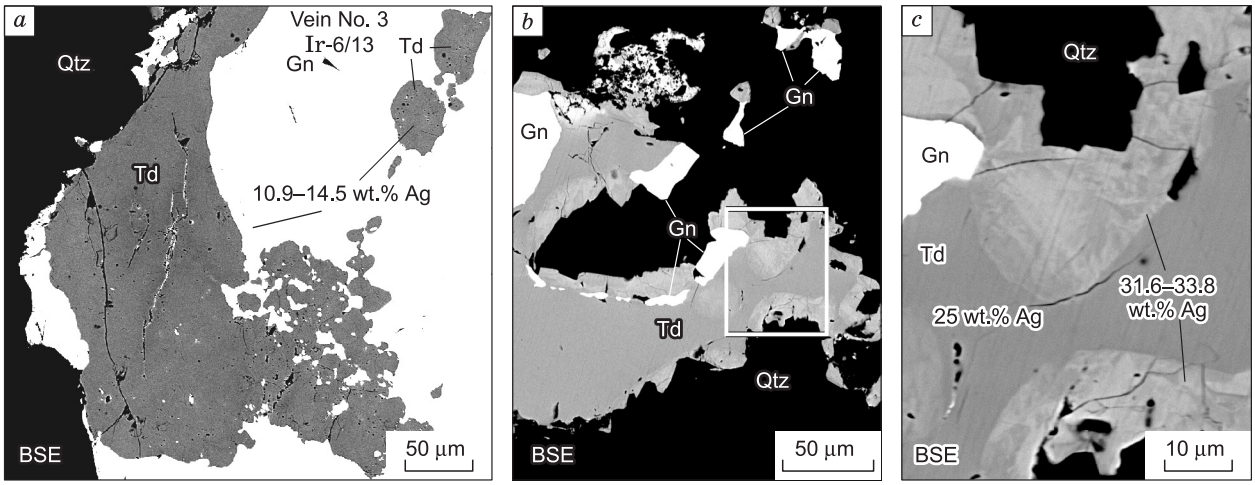

Fig. 8. Fahlore group minerals from the Irokinda deposit, Vein 3, sample Ir-6/13 (*a*), and from the Kedrovskoe deposit, Pineginskaya vein, sample K-26/15 (*b*, *c*).

wider range of Ag contents (20 to 35 wt.%, Table 4, ans. 16–22). Earlier, fahlores with a higher content of the tennantite end-member (*X*(As) of up to 0.28), domination of Zn over Fe, *X*(Fe) = 0.2–0.5, and Ag = 5–12 wt.% were found in assemblage with pyrite, sphalerite, and chalcopyrite (Fig. 9) in the Osinovaya vein (Bondar' et al., 2018).

Thus, we have established the compositional evolution of fahlores from the intermediate members of the tennantite–tetrahedrite series with similar Zn and Fe contents to Fe-tetrahedrites with high Ag contents and, then, to freibergites (Fig. 9).

Native gold. Native gold has been studied in Vein 3 and the Kvartsevaya and Serebryakovskaya veins of the Irokinda deposit, in the Osinovaya and Barguzinskaya veins of the Kedrovskoe deposit, and in one sample from the Vitimkon ore occurrence (Appendix B (http://sibran.ru/journals/Appendix B_27-06-18.xlsx)). Silver is the only impurity in native gold, and the contents of Hg and Cu are below their detection limits. Native gold of the KIOF shows an extremely wide range of fineness, 269–980 (Appendix B).

The widest variations in the composition of native gold have been established in the Irokinda deposit (from 269 to 907). The morphology and sizes of gold grains are also diverse: from visible grains (Fig. 2*e–g*) to microparticles (Figs. 4*d*, *e* and 10). In quartz, native gold grains are localized in the crystal interstices and therefore are often angular (Fig. 10*a*). Gold veinlets are often present in pyrite (Fig. 4*d*) and sphalerite, and rounded or oval gold particles usually occur in galena (Fig. 10*h*).

In *the Kvartsevaya vein*, irregular-shaped angular gold is present mainly in quartz and in intergrowth with pyrite but always in the immediate vicinity with galena (Fig. 10*c–h*). The gold is of high fineness (840–907), and its grains are usually chemically homogeneous.

In *Vein 3* and *the Serebryakovskaya vein*, gold occurs in assemblage with galena, either in intergrowth with it or in

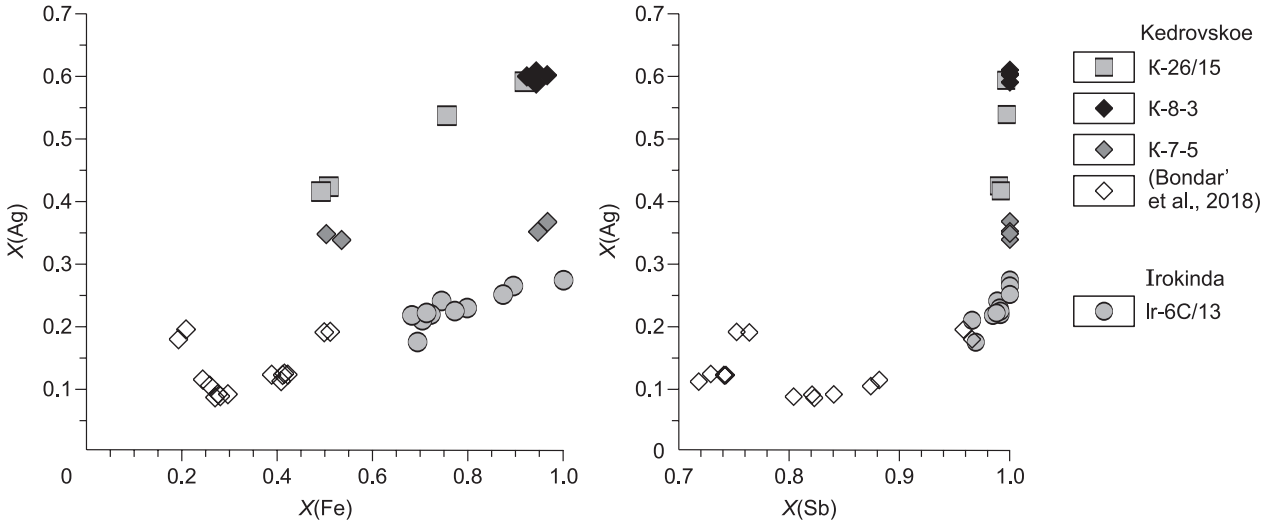

Fig. 9. *X*(Ag)–*X*(Fe) and *X*(Ag)–*X*(Sb) diagrams for fahlores of the KIOF (%).

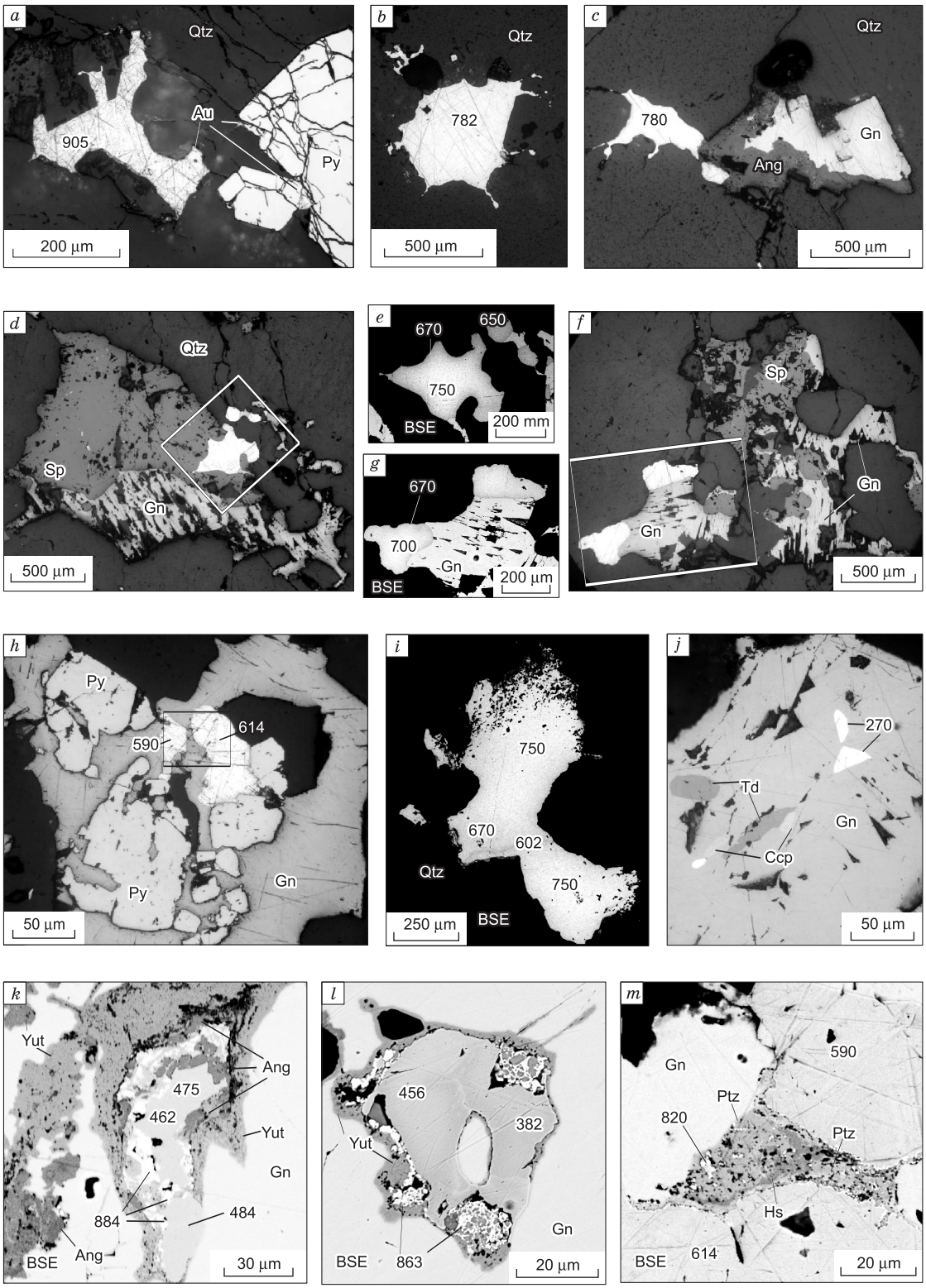

Fig. 10. Native gold of the Irokinda deposit. *a*, Kvartsevaya vein; *b*, *c*, Serebryakovskaya vein, sample Ir-87/13; *d–m*, Vein 3; numerals mark the fineness of gold. *a*, Native gold and pyrite in quartz, sample Ir-69/13; *b*, native gold in quartz; *c*, native gold intergrown with anglesite (Ang) replacing galena in quartz; *d*, native gold overgrowing sphalerite, sample Ir-15/13; *e*, enlarged fragment of *d*, native gold grains with a smooth zoning; *f*, native gold intergrown with galena; *g*, enlarged fragment of *f*, native gold grains with a smooth zoning; *h*, native gold intergrown with pyrite in galena, sample Ir-20/13; *i*, native gold of inhomogeneous composition in quartz, sample Ir-15/13; *j*, triangular segregations of native gold and tetrahedrite in galena, sample Ir-6/13; *k*, native low-fineness gold in galena and hypergene anglesite, yutenbogaardtite (Yut) and high-fineness gold; *l*, native low-fineness gold in galena and hypergene yutenbogaardtite and high-fineness gold; *m*, enlarged fragment of *h*, native low-fineness gold, galena, intergrowth of hessite and petzite (Ptz), and high-fineness gold.

Table 5. Chemical composition of sphalerite from the Irokinda (1–21) and Kedrovskoe (22–39) deposits, wt.% (electron probe microanalysis data), and FeS and CdS contents, mol%

No.	Sample, description	Zn	Cu	Fe	Cd	In	S	Total	FeS	CdS
1	Ir-15/13, large nests in quartz (Fig. 10*d*)	63.74	<D.l.	2.67	0.14	N.d.	34.16	100.71	4.67	0.12
2		63.78	<D.l.	3.04	0.09	N.d.	33.34	100.24	5.28	0.07
3		63.82	<D.l.	2.34	0.14	N.d.	33.21	99.50	4.10	0.13
4		64.04	0.04	2.56	0.12	N.d.	33.26	100.02	4.46	0.11
5		64.15	<D.l.	2.49	0.15	N.d.	33.76	100.56	4.34	0.13
6		64.17	<D.l.	2.50	0.16	N.d.	34.43	101.26	4.34	0.14
7	Ir-6C/13, oval grain in galena	65.23	0.23	1.14	0.24	N.d.	33.34	100.17	1.99	0.21
8		64.57	0.85	1.93	0.21	N.d.	33.66	101.22	3.32	0.18
9		65.18	0.10	0.86	0.20	N.d.	33.55	99.89	1.52	0.17
10	Ir-64/13, large grain, from edge to core	64.20	0.08	1.20	0.87	N.d.	34.46	100.81	2.12	0.77
11		63.81	<D.l.	1.64	0.85	N.d.	33.51	99.81	2.89	0.75
12		63.64	<D.l.	1.75	1.00	N.d.	33.28	99.67	3.09	0.88
13		63.26	<D.l.	1.87	0.84	N.d.	32.98	98.95	3.31	0.74
14		63.13	<D.l.	1.85	1.03	N.d.	33.43	99.43	3.28	0.91
15		63.04	<D.l.	2.31	0.92	N.d.	33.14	99.40	4.07	0.80
16	Ir-69/13, fine grain with galena in pyrite	62.66	<D.l.	3.43	0.90	N.d.	34.06	101.04	5.97	0.78
17		64.30	0.18	2.26	0.73	N.d.	33.87	101.33	3.92	0.62
18		61.86	2.13	3.09	0.64	N.d.	33.99	101.71	5.32	0.54
19		63.05	<D.l.	3.49	0.73	N.d.	33.39	100.66	6.05	0.62
20*	Ir-80/13, fine grain in galena (Fig. 5*h*)	62.38	<D.l.	3.33	<D.l.	N.d.	34.28	99.99	5.88	0.00
21*		63.84	<D.l.	3.11	<D.l.	N.d.	33.48	100.43	5.41	0.00
22	K-12/14, large grain, from core to edge	58.06	<D.l.	7.72	0.55	N.d.	34.32	100.67	13.40	0.48
23		57.68	<D.l.	7.76	0.68	N.d.	33.83	99.96	13.53	0.59
24		57.36	<D.l.	8.02	0.86	N.d.	33.72	99.95	13.96	0.75
25		57.54	<D.l.	7.83	0.67	N.d.	33.69	99.73	13.66	0.58
26		58.00	<D.l.	7.44	0.77	N.d.	33.80	100.02	12.97	0.67
27	K-12a/14, overgrows pyrite	62.46	<D.l.	3.01	0.81	N.d.	33.61	99.90	5.31	0.71
28		61.62	0.04	4.01	0.92	N.d.	33.73	100.32	7.02	0.80
29	K-13/15, large grain, from edge to edge	60.93	<D.l.	5.38	0.76	0.07	33.11	100.24	9.30	0.65
30		60.76	<D.l.	5.14	0.87	0.10	33.00	99.87	8.94	0.75
31		61.17	<D.l.	5.20	0.90	0.04	32.96	100.26	8.96	0.77
32		60.70	<D.l.	5.52	0.75	0.12	33.07	100.15	9.54	0.64
33		60.51	<D.l.	5.62	0.71	0.04	32.91	99.79	9.74	0.61
34	K-26/15, large grain, from edge to edge	61.81	0.11	4.00	0.68	0.07	33.03	99.70	6.99	0.59
35		60.42	0.06	5.37	0.66	0.09	33.06	99.67	9.36	0.57
36		60.09	0.05	5.68	0.60	0.06	33.23	99.71	9.89	0.52
37		59.40	0.04	5.46	0.68	0.10	33.26	98.95	9.64	0.60
38	K-26/15, fine grain with chalcopyrite	63.64	0.30	1.57	0.99	0.09	32.76	99.36	2.77	0.87
39		63.50	0.74	1.85	1.13	0.11	33.02	100.35	3.23	0.98

Note. N.d., Not determined; <D.l., below the detection limit.

the immediate vicinity of its grains. Galena often contains native-gold inclusions, usually rounded or oval with smooth edges, which indicates the nearly simultaneous formation of these minerals. The fineness of native gold varies from 755 to 382 in Vein 3 and from 783 to 589 in the Serebryakovskaya vein. In Vein 3, the largest (up to several hundred microns) gold grains have a smooth zoning; the fineness decreases from core to edges, with the difference in Ag contents being 3–6 wt.% and, locally, up to 15–16 wt.% (Fig. 10*e*–*g*). Sometimes, galena from Vein 3 has triangular segregations of küstelite ($Au_{17}Ag_{83}$) with a fineness of ~270 (Fig. 10*j*). Probably, they fill triangular pits in galena and formed later than this mineral (and, correspondingly, electrum of higher fineness).

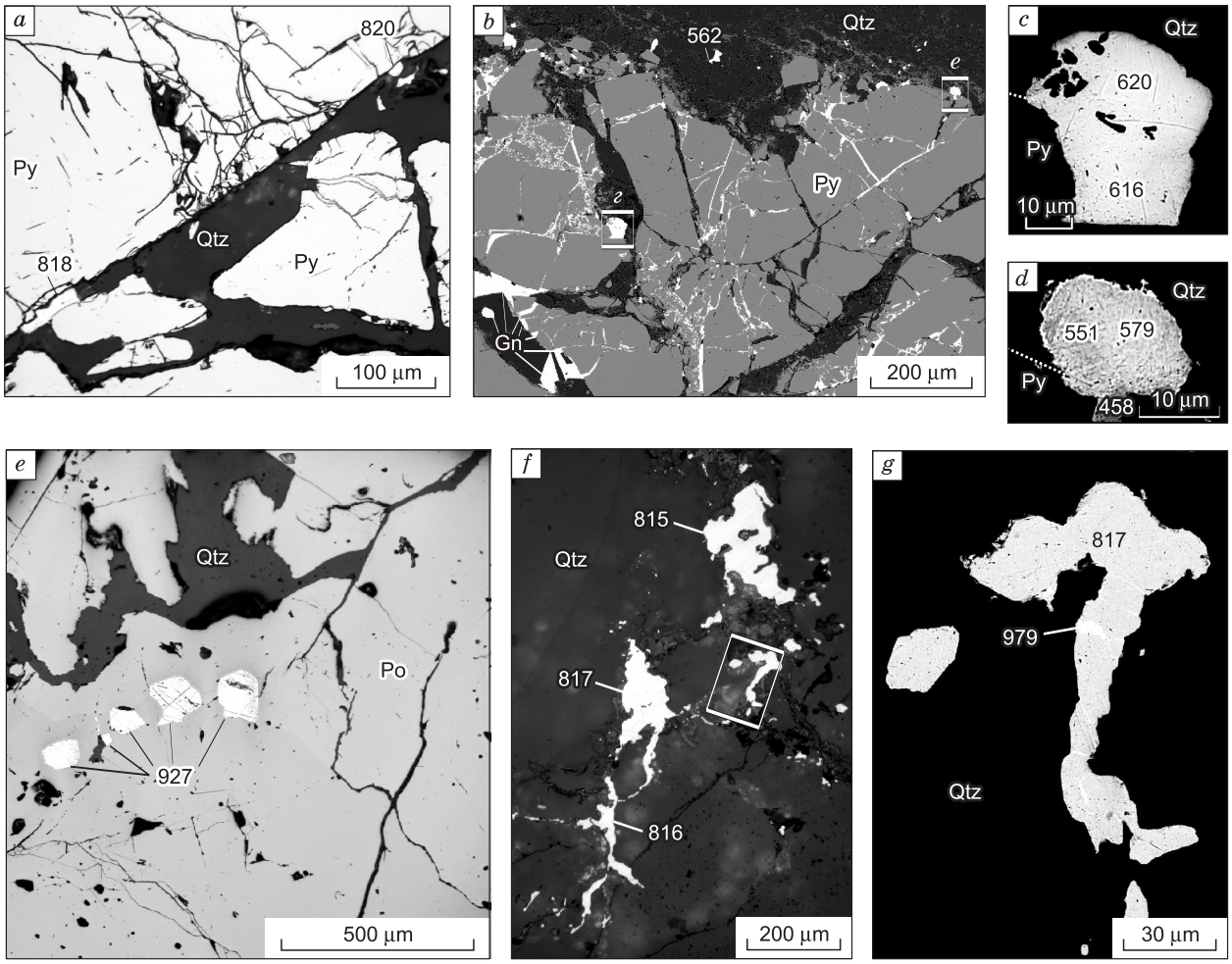

Fig. 11. Native gold/electrum from the Kedrovskoe deposit (*a*–*e*) and the Vitimkon ore occurrence (*f*, *g*). *a*, Native gold filling cracks in pyrite, sample K−12a/14; *b*, galena and native-gold stringers in pyrite, sample K-16/14; *c*, *d*, enlarged fragments of *b*, zoned native-gold grains; *e*, native high-fineness gold in pyrrhotite, sample B-1/15; *f*, amoeba-like native gold grains in quartz, sample Vit-1; *g*, enlarged fragment of *f*, hypergene(?) stringers of native high-fineness gold.

In *Vein 3* (Fig. 10*k*, *l*), *hypergene* native gold (881–886) was also found. It forms discontinuous ~10 μm wide rims around electrum (382–484) at the sites where the latter is replaced by yutenbogaardtite (Ag_3AuS_2). According to Palyanova et al. (2014), this mineral assemblage is specific to hypergene sulfidization of low-fineness electrum (380–650). We tentatively consider gold (821–863) from the samples Ir-6C/13 and Ir-20/13 hypergene, resulted from the decomposition of petzite (Fig. 10*m*).

In **the Kedrovskoe deposit**, the Ag content in native gold shows less significant variations, and the gold fineness is, in general, slightly higher (929–458). We studied native gold of the Osinovaya vein more thoroughly. In mineral assemblages and chemical composition it is similar to gold of Vein 3 (Figs. 10 and 12, Appendix B). Gold overgrows pyrite and fills cracks and pores in it (Fig. 11*a*). The fineness of gold is 805–820. Native gold in assemblage with galena also filling cracks and pores in pyrite (Fig. 11*b*–*d*) is of lower fineness (620–458). It has a homogeneous chemical composition, but some grains have a smooth chemical zoning (Fig. 11*d*, *e*), with fineness varying from 579 to 458.

In *the Barguzinskaya vein*, native gold occurs as isometric segregations in pyrrhotite (Fig. 11*f*) and is characterized by high fineness (926–929).

In **the Vitimkon ore occurrence,** gold was found only in quartz (Fig. 11*g*), where it is present as amoeba-like segregations up to 200 μm in size and has fineness of 812–820. Sometimes it contains fine (less than few microns) stringers of gold of higher fineness (864–979), most likely, hypogene (Figs. 11*h* and 12*b*, Appendix B).

Thus, we have established the evolution of the chemical composition of hypogene native gold in the KIOF, namely, a gradual increase in the content of Ag from early to late gold generations.

Sphalerite. Sphalerite occurs as isometric segregations in vein quartz. The segregations measure up to few millimeters and, sometimes, few centimeters (*Kvartsevaya vein* and *Vein 3* in **the Irokinda deposit** and *Osinovaya vein* in **the**

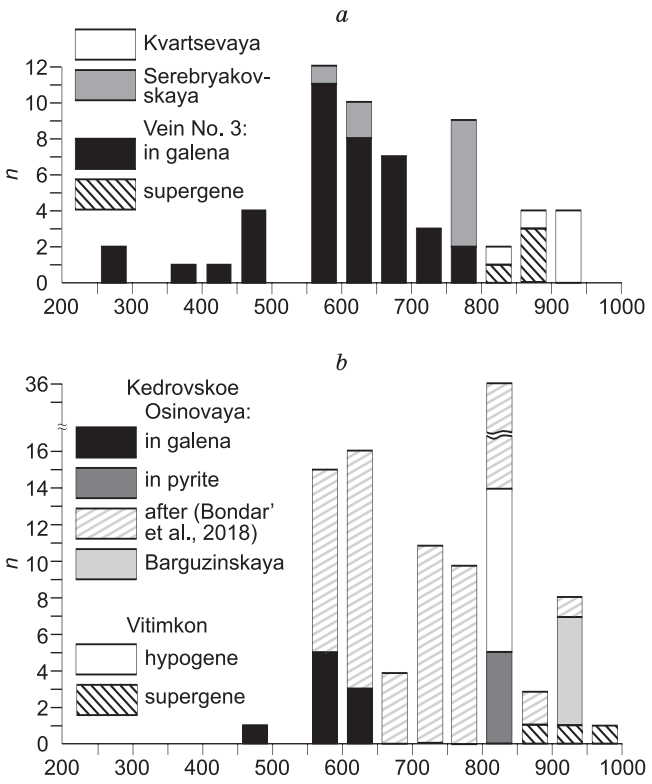

Fig. 12. Histograms of the fineness of native gold from the Irokinda deposit (*a*) and the Kedrovskoe deposit and Vitimkon ore occurrence (*b*). *n*, occurrence, units.

Kedrovskoe deposit (sample K-13/15)) (Fig. 2*d*). It is also present as oval grains few hundred microns in size in later formed galena (*Serebryakovskaya vein* and *Vein 3*) (Figs. 4*e* and 6*b*) and sometimes cements earlier formed pyrite (Kedrovskoe deposit, Osinovaya vein) (Fig. 4*c*). Sphalerite is usually rich in disseminated emulsion of chalcopyrite (Fig. 5*h*) or, more seldom, pyrrhotite.

Iron and cadmium are the main impurities in sphalerite; the contents of Hg, Mn, Sb, and Sn are below their detection limits. The contents of Cu do not exceed its detection limit but reach 2.1 wt.% in sphalerite with trapped chalcopyrite. Sphalerite from *Vein 3* contains 1.5–5.3 mol % FeS and 0.1–0.2 mol % CdS (Table 5, ans. 1-9; Fig. 13). Sphalerite from *the Serebryakovskaya vein*, analyzed only by energy-dispersive spectroscopy, has a similar composition (Table 5, ans. 20–21; Fig. 13). Sphalerite from *the Kvartsevaya vein* has similar contents of FeS (2.1–6.0 mol %) and significantly higher contents of CdS (0.5–0.9 mol %) (Table 5, ans. 10–19).

In *the Osinovaya vein* of **the Kedrovskoe deposit**, sphalerite is much richer in Fe. The largest crystals (from few millimeters to few centimeters) contain pyrrhotite dissemination and have FeS ≤ 13–14 mol % and CdS = 0.5–0.7 mol % (Table 5, ans. 22–26). The smaller crystals with disseminated chalcopyrite emulsion have FeS = 5.3–7.0 mol % and CdS = 0.7–0.8 mol % (Table 5, ans. 27–28). In *the Pineginskaya vein*, coarse sphalerite crystals also have higher FeS contents as compared with the small crystals, 7–10 and 2.8–3.2 mol %, respectively, whereas their CdS contents are, on the contrary, lower, 0.5–0.6 and 0.9–1.0 mol % (Table 5, ans. 34–39).

The contents of impurity elements within the large sphalerite grains show no significant variations.

DISCUSSION

Trace elements **in galena.** Comparison of probe microanalysis results with LA-ICP-MS data shows agreement in the Ag, Bi, and Se contents, whereas the Sb contents determined by LA-ICP-MS are approximately 1.5–2 times higher than those estimated by probe microanalysis (sample K-19/14). This might be due to Sb mineral inclusions, which we could not take into account, or to the imperfect standard used. Nevertheless, the obtained LA-ICP-MS data can be used to discuss the relative variations in the contents of trace elements.

We analyzed correlations among the contents of Cu, Zn, As, Se, Ag, Cd, Sn, Sb, Te, Tl, and Bi, because the contents of the other elements did not exceed their detection limits in

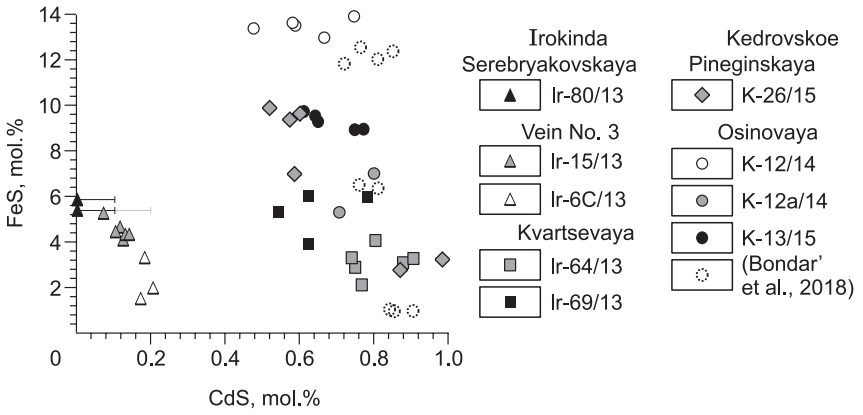

Fig. 13. FeS–CdS diagram for sphalerite from the Kedrovskoe–Irokinda ore field.

Table 6. Coefficients of pair correlation for trace elements in galena

Element	Cu	Zn	As	Se	Ag	Cd	Sn	Sb	Te	Tl	Bi	Sb + Bi
Cu	1											
Zn	–0.34	1										
As	–0.16	0.18	1									
Se	**0.81**	–0.19	0.13	1								
Ag	**0.89**	–0.22	–0.01	**0.66**	1							
Cd	0.05	0.22	0.19	–0.27	0.39	1						
Sn	–0.40	0.31	–0.23	**–0.62**	–0.39	0.31	1					
Sb	0.12	0.07	0.51	0.10	0.52	**0.73**	–0.14	1				
Te	**0.78**	–0.17	–0.48	0.57	0.47	–0.31	–0.16	–0.49	1			
Tl	–0.04	0.28	0.25	0.24	–0.15	–0.51	–0.04	–0.25	0.19	1		
Bi	**0.84**	–0.26	–0.42	**0.64**	0.57	–0.29	–0.29	–0.40	**0.98**	0.13	1	
Sb + Bi	**0.84**	–0.16	0.13	**0.64**	**0.99**	0.45	–0.38	**0.62**	0.38	–0.14	0.48	1
For all samples, except for Ir-69/13 and K-19/14 (n = 9)												
Cu	1											
Zn	–0.22	1										
As	**0.62**	0.16	1									
Se	**0.80**	0.10	0.49	1								
Ag	–0.47	0.38	0.06	–0.34	1							
Cd	**–0.61**	0.40	–0.15	**–0.78**	0.41	1						
Sn	–0.57	0.22	–0.35	–0.58	–0.23	0.54	1					
Sb	–0.29	0.54	0.37	–0.24	**0.91**	0.48	–0.14	1				
Te	–0.27	0.39	–0.29	–0.01	–0.48	0.07	**0.67**	–0.37	1			
Tl	0.12	0.28	0.46	0.49	–0.03	–0.44	–0.08	0.10	0.36	1		
Bi	0.48	–0.37	0.15	**0.64**	–0.09	**–0.88**	**–0.65**	–0.17	–0.29	0.31	1	
Sb + Bi	–0.24	0.50	0.40	–0.17	**0.91**	0.39	–0.21	**0.99**	–0.41	0.14	–0.06	1

Note. For all samples n = 11. Coefficients of pair correlation were calculated using the geometric mean of element contents in each sample (see Table 3). When it was impossible to calculate the geometric mean, the value equal to half the detection limit was used. The correlation coefficients of >0.6 are significant (a confidence level of 0.05 was taken) and are bold-typed. The significant coefficients established for both samples are underlined.

more than a half of the analyses. In most of the correlation diagrams (Fig. 14), each sample forms a compact field virtually not overlapping with the fields of other samples. Since most of the trace elements show a discrete distribution and different samples are characterized by different numbers of analyses, the coefficients of pair correlations were calculated for the geometric means for each sample. The calculation was made for the entire set of the samples and for the set with the rejected samples Ir-69/13 and K-19/14 (Table 6), which differ significantly from the rest samples in the contents of some elements (Fig. 14*a*, *b*, *d*, *f*). This approach was applied to establish steadily significant correlations (significant correlations coinciding in both sets of the samples), hereinafter referred to as correlations.

The high positive correlation between the contents of Sb and Ag established for most samples (Fig. 14*a*; Table 6) is due to the isomorphic incorporation of these elements into galena according to the scheme $Ag^{+} + Sb^{3+} \leftrightarrow 2Pb^{2+}$ (Chutas et al., 2008; Renock and Becker, 2011). Excess Sb can isomorphically enter galena with the appearance of vacancies: $2(Sb)^{3+} + \square$ (vacancy) $\leftrightarrow 3Pb^{2+}$ (George et al., 2015).

In the sample Ir-69/13 (Kvartsevaya vein, Irokinda deposit) with a minor content of Sb and Bi > 3000 ppm, the isomorphic substitution $Ag^{+} + (Bi^{3+}) \leftrightarrow 2Pb^{2+}$ (Chutas et al. 2008; Renock and Becker, 2011) seems to take place. This is confirmed by a high positive correlation (0.99) between the contents of Ag and Sb + Bi (Table 6). Apparently, As^{3+}, Cu^{+}, and Tl^{+} can be incorporated into galena by the same scheme (George et al., 2015).

As seen from Table 6, Ag and Sb show no correlation with Zn and As, which indirectly confirms that these elements are isomorphically incorporated into galena lattice but do not form inclusions of sulfosalts, such as fahlores, which always contain As, Fe, and Zn. The absence of Te–Ag correlation (Fig. 14*f*) indicates the lack of inclusions of hessite or Te-containing Ag sulfosalts (polybasite and can-

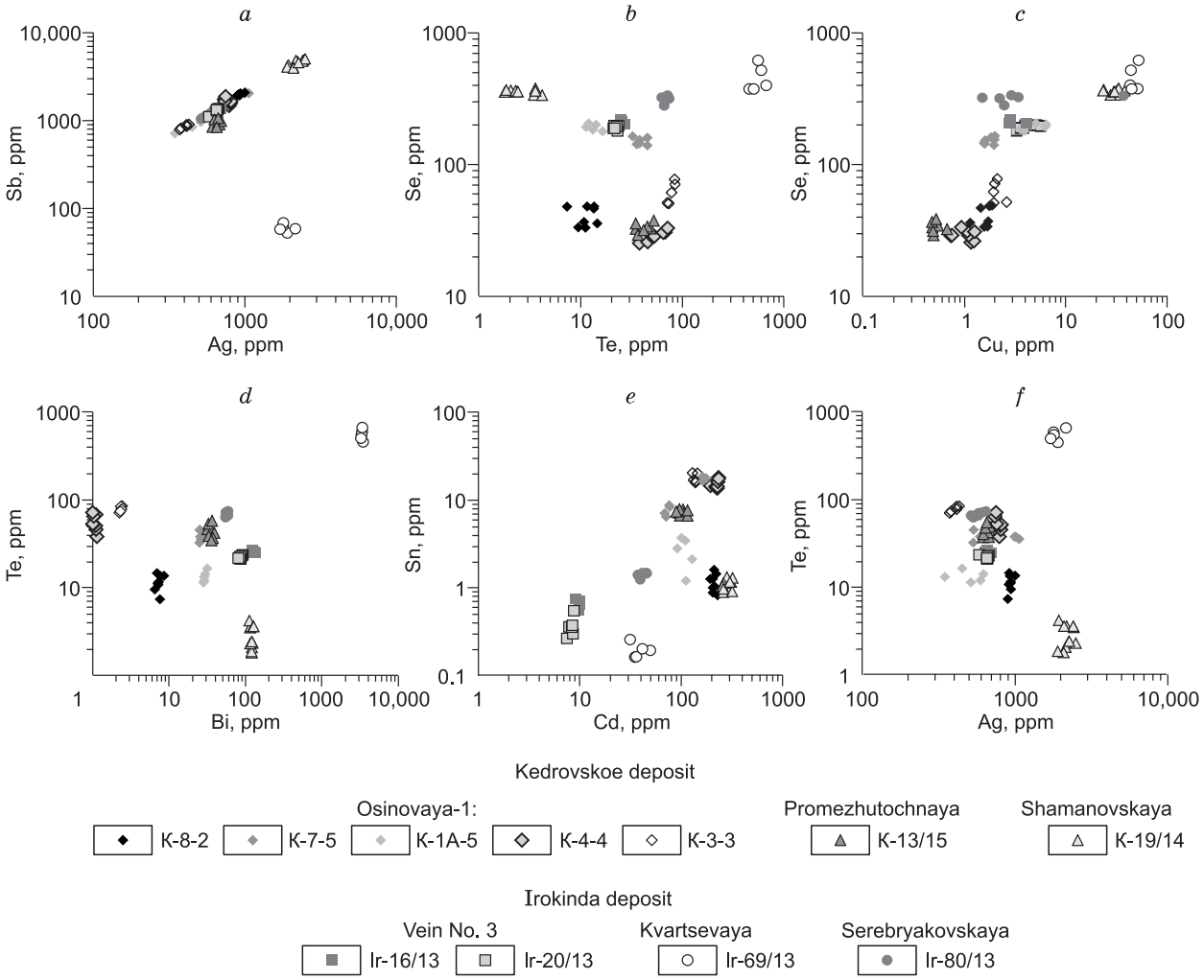

Fig. 14. Binary plots for trace elements in galena (from LA–ICP-MS data).

fieldite). The absence of Bi–Te correlation in galena (sample Ir-69/13) confirms that tetradymite found in this sample was not trapped during LA-ICP-MS analysis (Fig. 5*e*).

Divalent metals (Cd and Zn) can isomorphically substitute Pb^{2+} (Blackburn and Schwendeman, 1977). The absence of a positive correlation between these elements indirectly indicates the absence of sphalerite inclusions. There is also no correlation between the contents of Te and Se (Fig. 14*b*), i.e., these metals isomorphically replace sulfur independently of each other. There are positive Se–Cu (Fig. 14*c*) and Se–Bi (Table 6) correlations, which can be related to the isomorphism $PbS \leftrightarrow CuBiSe_2$.

There are few literature data on the chemical composition of galena established by local high-sensitivity methods (Blackburn and Schwendeman, 1977; Reeson et al., 1990; George et al., 2015). Data on the chemical composition of galena of orogenic gold deposits are also scarce (Hastie et al., 2018). Note that the significant element correlations that we have established were not reported by George et al. (2015), who studied trace elements in galena from skarn, porphyry, epithermal, and SEDEX deposits. On the other hand, the pair correlations considered in the above research (Bi–Ag, Te–Ag, Bi–Te, and Bi–Ag) are not observed in the KIOF galena; the only exception is the positive (Sb + Bi)–Ag correlation. This indicates the specific trace-element composition of galena of orogenic gold deposits.

Traces of gold (up to 0.5 ppm) have been found only in galena of the samples K-19/14 and Ir-80/13. The samples lack microscopically visible native gold grains. However, the uneven distribution of Au in the galena grains (Fig. 6*h*) suggests the presence of native gold nanoinclusions.

Mineral composition of ores. The diversity of Ag minerals (sulfosalts (tetrahedrite (Ag), polybasite (Te), diaphorite, and canfieldite (Te)) and tellurides (hessite, petzite, stützite, and empressite) is a rare phenomenon in orogenic deposits, although in Mother Lode (Weir and Kerrick, 1987), Kumtor (Ivanov et al., 2000), Zun-Kholba (Brazhnik, 1993), and some other gold deposits gold and silver tellurides are widespread and make a significant contribution to the balance of precious metals. Occasional findings of can-

fieldite (Te) are known in the Nikolaevskoe gold deposit, Yenisei Ridge (Safina et al., 2015), and silver tellurides were discovered in the Bodaibo synclinorium deposits (Distler et al., 2004; Palenova et al., 2015).

The widely ranging fineness of the KIOF native gold is also rare in orogenic deposits. Most often, gold has fineness of 850–900 (Morrison et al., 1991; Ridley et al., 1996; Cassidy et al., 1998). In some deposits, however, native gold shows a wide variation in composition, e.g., gold of the Bohaun deposit contains up to 40 wt.% Ag (Lusty et al., 2011), late electrum (in assemblage with galena) of the Krasnoe ore occurrence has fineness of 565–649 (Palenova et al., 2015), and gold of the Zun-Kholba deposit (East Sayan) shows a decrease in fineness from 950 in the early generation to 250 in the late one (Brazhnik, 1993). Such variations in native-gold composition are more common in deposits of other genetic types, e.g., epithermal (Morrison et al., 1991), porphyry, or skarn (Gas'kov, 2017) ones, i.e., deposits with significant variations in the physicochemical conditions of ore formation. Usually, a decrease in gold fineness is associated with a decrease in temperature and sulfur and(or) oxygen fugacity during the mineral formation (Palyanova, 2008). The distribution of the KIOF gold fineness shows three distinct peaks (Fig. 12): in the ranges 550–650, 750–850, and 850–950. A similar fineness distribution pattern was earlier established for native gold of the Yurasovskaya-II vein of the Irokinda deposit (Khrustalev and Khrustaleva, 2006) and of the Osinovaya vein (Bondar' et al., 2018). The compositional variations and type of zoning indicate that gold was deposited almost continuously for a long time on the background of jumpwise changes in physicochemical conditions.

The wide variations in Fe content in sphalerite (from 14 to 2.8 mol % FeS in the Kedrovskoe deposit and to 1.5 mol % FeS in the Irokinda deposit), like the variations in the native-gold composition, can be explained by a decrease in temperature and sulfur fugacity (Vaughan and Craig, 1978). The CdS contents, on the contrary, show narrow variations in each studied vein (Fig. 13). The solubility of Cd (and, correspondingly, its incorporation into sphalerite) depends directly on temperature, the chloride ion activity, and the Cd/Zn ratio in the fluid (Bazarkina, 2010; Bazarkina et al., 2010). However, we did not reveal any significant temporal variations in CdS content. The content of Cd in sphalerite usually varies negligibly within the same deposit (Cook et al., 2009). It was assumed that this parameter is constant for each deposit and can be used to identify its genetic type (Qian, 1987; Wen et al., 2016). The Cd/Zn ratio was proposed to be used as an indicator of the source of fluid (Grichuk, 2005). Apparently, the Cd content in the KIOF sphalerite depends considerably on the composition of the host rocks, which governed the Cd/Zn ratio in the fluid. The lowest contents of Cd (0.1–0.2 wt.%) have been established in sphalerite of veins localized in Archean schists of the South Muya block (Vein 3 and Serebryakovskaya vein), whereas sphalerite of veins from Neoproterozoic rocks (Kvartsevaya vein of the Irokinda deposit and veins of the Kedrovskoe deposit) of different compositions has high contents of Cd (0.6–1.0 wt.%).

Similar behavior of Cd is observed in galena. The lowest contents of Cd (7.5–10 ppm) are found in Vein 3; its contents in the Kvartsevaya and Serebryakovskaya veins of the Irokinda deposit are somewhat higher (32–50 ppm). The Osinovaya and Shamanovskaya veins of the Kedrovskoe deposit, localized in the Neoproterozoic metasedimentary rocks of the Parama Group, have Cd = 69–324 ppm, with contents of 100–260 ppm prevailing. The distribution of Sn is similar: up to 0.7 ppm in the veins of the Irokinda deposit and up to 20 ppm in the veins of the Kedrovskoe deposit (Table 3, Fig. 14). This, along with the discrete distribution of almost all trace elements in galena (see above), indicates that the chemical composition of the mineral was determined primarily by the composition of fluid, which, in turn, might have been influenced by the chemical composition of the host rocks.

The key role of the lithologic and geochemical compositions of the host rocks is noted in many publications concerned with the genesis of orogenic gold deposits (Albers, 1981; Groves et al., 2003; Frei et al., 2009; Standish et al., 2014; Pitkairn et al., 2015; Chugaev and Chernyshev, 2017). At the same time, the interaction of fluid with the host rocks is treated as one of the main mechanisms of the supply of ore components into hydrothermal solutions. Study of the isotope composition of Sr, Nd, and Pb in the Kedrovskoe deposit showed that the rocks composing the Neoproterozoic juvenile crust in the BMOB were the source of the mineral-forming components of fluid (Chugayev et al., 2017). In the Muya segment of the BMOB, the volcanosedimentary rocks of the Ust'-Kelyana Formation, referred to as an island-arc association, are widespread. These rocks show high contents of Au relative to its Clarke contents (Vanin et al., 2017) and can be considered one of the potential sources of the ore components of fluid. Island arc volcanics were also found in the areas of the Mother Lode and Zun-Kholba deposits, which are similar in the mineral and geochemical compositions of ores to the KIOF gold deposits (Albers, 1981; Gordienko et al., 2016).

CONCLUSIONS

The studied KIOF ore veins are, in general, of similar mineral composition. Their mineralization formed within one ore stage and comprises quartz–pyrite and gold–sphalerite–galena (galena, sphalerite, fahlore, and native gold) assemblages (formed at different substages).

Hypogene native gold shows wide variations in composition (fineness of 929 to 270) and, often, a smooth zoning, which indicates that it was deposited almost continuously throughout the ore stage.

We have established the compositional evolution of fahlores from intermediate members of the tennantite–tetrahedrite series, with similar Zn and Fe contents, to Fe-tetrahedrites with high Ag contents (>10 wt.%) and, then, to freibergites (>30 wt.% Ag).

Numerous inclusions of Ag-minerals (polybasite (Te), diaphorite, canfieldite (Te), petzite, stützite, and empressite), tetradymite, and ulmanite have been found in galena.

According to the LA–ICP-MS data, Sb and Ag are major trace elements in the KIOF galena; there are also Bi, Se, Cd, Te, Cu, Zn, As, and Sn. The contents of trace elements vary significantly from sample to sample and are often in correlation with the composition of the host rocks.

According to the EPMA data, sphalerite from veins localized in the South Muya block schists is poorer in Cd (0.1–0.2 wt.%) than sphalerite from veins in Neoproterozoic rocks of different compositions (0.6–1.0 wt.% Cd).

In general, the KIOF gold ore veins are a rare example of orogenic deposits with a diversity of precious-metal minerals and a wide range of the compositions of native gold and other ore minerals, which is primarily due to the different compositions of the host rocks.

We thank V.I. Nazarov and Kh.Kh. Muratshin (Zapadnaya Gold Mining Ltd) and G.N. Shulyak (Buryatzoloto PJSC) for assistance in the field works, as well as N.N. Koshlyakova (Lomonosov Moscow State University), E.V. Koval'chuk, I.G. Griboedova, A.N. Nekrasov, S.E. Borisovskii, and V.I. Taskaev (Institute of Geology of Ore Deposits, Petrography, Mineralogy and Geochemistry, Moscow) for the analyses. We are sincerely grateful to E.A. Naumov and an anonymous reviewer for valuable critical remarks.

The work was performed on the state assignment (project 0136-2014-0006) with partial financial support by grant 16-35-60033 from the Russian Foundation for Basic Research.

REFERENCES

Albers, F.J.P., 1981. A lithologic-tectonic framework for the metallogenic provinces of California. Econ. Geol. 76 (4), 1411–1429.

Bazarkina, E.F., 2010. Transfer of Cadmium and Zinc by Hydrothermal Fluids: Experiment and Physicochemical Modeling. PhD Thesis [in Russian]. IGEM RAN, Moscow.

Bazarkina, E.F., Zotov, A.V., Akinfiev, N.N., 2010. Pressure-dependent stability of cadmium chloride complexes: potentiometric measurements at 1–1000 bar and 25 ºC. Geol. Ore Deposits 52 (2), 167–178.

Bazhenov, V.I., Gribanov, A.P., Rubanov, V.A., Dul'zon, O.A., 1970. Near-vein alterations of host rocks at the contacts of gold–quartz veins in the Irokinda ore field. Izvestiya Tomskogo Politekhnicheskogo Instituta 218, 15–21.

Bindi, L., Nestola, F., Guastoni, A., Zorzi, F., Peruzzo, L., Raber, T., 2012. Te-rich canfieldite, $Ag_8Sn(S,Te)_6$, from the Lengenbach Quarry, Binntal, Canton Valais, Switzerland: Occurrence, description and crystal structure. Can. Mineral. 50, 111–118.

Bindi, L., Voudouris, P., Spry, P.G., 2013. Structural role of tellurium in the minerals of the pearceite–polybasite group. Mineral. Mag. 77, 419–428.

Blackburn, W.H., Schwendeman, J.F., 1977. Trace element substitution in galena. Can. Mineral. 15, 365–377.

Bondar', D.B., Chugaev, A.V., Polekhovskii, Yu.S., Koshlyakova, N.N., 2018. The ore mineralogy of the Kedrovskoe gold deposit (the Muya region, the Republic of Buryatia, Russia). Moscow University Geology Bulletin 73 (4), 380–389.

Brazhnik, A.V., 1993. Zun-Kholba gold deposit (Buryatia). Rudy i Metally, Nos. 3–6, 80–90.

Buryak, V.A., 1982. Metamorphism and Ore Formation [in Russian]. Nedra, Moscow.

Cassidy, K.F., Groves, D.I., McNaughton, N.J., 1998. Late-Archean granitoid-hosted lode-gold deposits, Yilgarn Craton, Western Australia: Deposit characteristics, crustal architecture and implications for ore genesis. Ore Geol. Rev. 13, 65–102.

Chugaev, A.V., Chernyshev, I.V., 2017. Pb–Pb isotopic systematics of orogenic gold deposits of the Baikal–Patom Fold Belt (Northern Transbaikalia, Russia) and estimation of the role of Neoproterozoic crust in their formation. Geochem. Int. 55 (11), 1010–1021.

Chugaev, A.V., Plotinskaya, O.Yu., Chernyshev, I.V., Lebedev, V.A., Belogub, E.V., Goltsman, Yu.V., Larionova, Yu.O., Oleinikova, T.I., 2017. Age and sources of matter for the Kedrovskoe gold deposit, northern Transbaikal region, Republic of Buryatia: geochronological and isotopic geochemical constraints. Geol. Ore Deposits 59 (4), 281–295.

Chutas, N.I., Kress, V.C., Ghiorso, M.S., Sack, R.O., 2008. A solution model for high-temperature $PbS–AgSbS_2–AgBiS_2$ galena. Am. Mineral. 93 (10), 1630–1640.

Cook, N.J., Ciobanu, C.L., Pring, A., Skinner, W., Shimizu, M., Danyushevsky, L., Saini-Eidukat, B., Melcher, F., 2009. Trace and minor elements in sphalerite: A LA-ICP-MS study. Geochim. Cosmochim. Acta 73 (16), 4761–4791.

Distler, V.V., Yudovskaya, M.A., Prokof'ev, V.Yu., Lishnevskii, E.N., Mitrofanov, G.L., 2004. Geology, composition, and genesis of the Sukhoi Log precious metals deposit, Russia. Ore Geol. Rev. 24, 7–44.

Frei, R., Dahl, P.S., Frandsson, M.M., Jensen, L.A., Hansen, T.R., Terry, M.P., Frei, K.M., 2009. Lead-isotope and trace-element geochemistry of Paleoproterozoic metasedimentary rocks in the Lead and Rochford basins (Black Hills, South Dakota, USA): Implications for genetic models, mineralization ages, and sources of leads in the Homestake gold deposit. Precambrian Res. 172 (1-2), 1–24.

Gas'kov, I.V., 2017. Major impurity elements in native gold and their association with gold mineralization settings in deposits of Asian folded areas. Russian Geology and Geophysics (Geologiya i Geofizika) 58 (9), 1080–1092 (1359–1376).

George, L., Cook, N.J., Ciobanu, C.L., Wade, B., 2015. Trace and minor elements in galena: A reconnaissance LA-ICP-MS study. Am. Mineral. 100, 548–569.

Goldfarb, R.J., Groves, D.I., 2015. Orogenic gold: Common or evolving fluid and metal sources through time. Lithos 233, 2–26.

Goldfarb, R.J., Taylor, R.D., Collins, G.S., Goryachev, N.A., Orlandini, O.F., 2014. Phanerozoic continental growth and gold metallogeny of Asia. Gondwana Res. 25 (1), 48–102.

Gordienko, I.V., Roshchektaev, P.A., Gorokhovsky, D.V., 2016. Oka ore district of the Eastern Sayan: geology, structural–metallogenic zonation, genetic types of ore deposits, their geodynamic formation conditions, and outlook for development. Geol. Ore Deposits 58 (5), 361–382.

Grichuk, D.V., 2005. The Cd/Zn ratio as an indicator of the contribution of magmatic fluids to the feeding of hydrothermal systems, in: Proceedings of the Seventh International Conference "New Ideas in Geosciences" [in Russian]. Moscow, Vol. 2, p. 83.

Groves, D.I., Goldfarb, R.J., Gebre-Mariam, M., Hagemann, S.G., Robert, F., 1998. Orogenic gold deposits: A proposed classification in the context of their crustal distribution and relationship to other gold deposit types. Ore Geol. Rev. 13, 7–27.

Groves, D.I., Goldfarb, R.J., Robert, F., Hart, G.J.R., 2003. Gold deposits in metamorphic belts: overview of current understanding,

outstanding problems, future research, and exploration significance. Econ. Geol. 98, 1–29.

Gusev, G.S., Khain, V.E., 1995. On relations between the Baikal–Vitim, Aldan–Stanovoy, and Mongol–Okhotsk terranes (south of mid-Siberia). Geotektonika, No. 5, 68–82.

Hastie, E.C.G., Gagnon, J.E., Samson, I.M., 2018. The Paleoproterozoic MacLellan deposit and related Au–Ag occurrences, Lynn Lake greenstone belt, Manitoba: An emerging, structurally-controlled gold camp. Ore Geol. Rev. 94, 24–45.

Ivanov, S.M., Ansdell, K.M., Melrose, D.L., 2000. Ore texture and stable isotope constraints on ore deposition mechanisms at the Kumtor lode gold deposit, in: Bucci, L.A., Mair, J.L. (Eds.), Gold in 2000. Littleton, Society of Economic Geologists, Poster Session Extended Abstracts Volume, pp. 47–52.

Kerrich, R., Cassidy, K.F., 1994. Temporal relationships of lode-gold mineralization to accretion, magmatism, metamorphism, and deformation—Archean to present: A review. Ore Geol. Rev. 9, 263–310.

Khrustalev, V.K., Khrustaleva, A.V., 2006. Gold Ore Metasomatites in Transbaikalia: Chemical Composition and Evaluation of Gold Resources [in Russian]. BNTs SO RAN, Ulan-Ude.

Kucherenko, I.V., 1989. Late Paleozoic epoch of gold mineralization in the Precambrian framing of the Siberian Platform. Izvestiya Akad. Nauk SSSR. Ser. Geol., No. 6, 90–102.

Kucherenko, I.V., 2004. Petrological and metallogenic implications of study of small intrusions in mesothermal gold ore fields. Izvestiya Tomskogo Politekhnicheskogo Universiteta 307 (1), 49–57.

Kucherenko, I.V., 2006a. Geochemical features of near-vein metasomatism in quartz diorites and granitoids of the domal structure of the Kedrovskoe gold deposit (northern Transbaikalia). Part 1. Conditions of occurrence and identification of igneous rocks. Izvestiya Tomskogo Politekhnicheskogo Universiteta 309 (2), 41–45.

Kucherenko, I.V., 2006b. Geochemical features of near-vein metasomatism in quartz diorites and granitoids of the domal structure of the Kedrovskoe gold deposit (northern Transbaikalia). Part 2. Metasomatic and geochemical aureoles around veins. Izvestiya Tomskogo Politekhnicheskogo Universiteta 309 (3), 22–26.

Kucherenko, I.V., 2014. Petrology of hydrothermal metasomatism of intermineral dike dolerites at mesothermal gold deposits. Part 1. Kedrovskoe deposit (northern Transbaikalia). Izvestiya Tomskogo Politekhnicheskogo Universiteta 325 (1), 155–165.

Lyakhov, Yu.V., Popivnyak, I.V., 1977. Physicochemical conditions of generation of gold mineralization in northern Buryatia. Izvestiya Akad. Nauk SSSR. Ser. Geol., No. 6, 9–18.

Lusty, P.A., Naden, J., Bouch, J.J., Mckervey, J.A., Mcfarlane, J.A., 2011. Atypical gold mineralization in an orogenic setting—The Bohaun deposit, western Irish Caledonides. Econ. Geol. 106 (3), 359–380.

Mitrofanov, L.F., Mikov, A.D., Rubanov, V.A., Gribanov, A.P., 1970. Mineralogy of gold deposits of the South Muya Ridge. Izvestiya Akad. Nauk SSSR. Ser. Geol. 218, 33–40.

Morrison, G.W., Rose, W.J., Jaireth, S., 1991. Geological and geochemical controls on the silver content (fineness) of gold in gold–silver deposits. Ore Geol. Rev. 6 (4), 333–364.

Nordgold, 2018. https://www.nordgoldjobs.com/about-company/irokinda-respublika-buryatiya.

Ondruš, P., Veselovský, F., Gabašová, A., Hloušek, J., Šrein, V., Vavrín, I., Skála, R., Sejkora, J., Drábek, M., 2003. Primary minerals of the Jáchymov ore district. J. Czech Geol. Soc. 48, 19–147.

Palenova, E.E., Blinov, I.A., Zabotina, M.V., 2015. Silver minerals from quartz veins of the Krasnoe deposit (Bodaibo ore region). Mineralogy, No. 2, 9–17.

Palyanova, G., 2008. Physicochemical modeling of the coupled behavior of gold and silver in hydrothermal processes: Gold fineness, Au/Ag ratios and their possible implications. Chem. Geol. 255, 399–413.

Palyanova, G., Karmanov, N., Savva, N., 2014. Sulfidation of native gold. Am. Mineral. 99, 1095–1103.

Paton, C., Hellstrom, J., Paul, B., Woodhead, J., Hergt, J., 2011. Iolite: Freeware for the visualisation and processing of mass spectrometric data. J. Anal. At. Spectrom. 26, 2508–2518.

Pitcairn, I.K., Craw, D., Teagle, D.A.H., 2015. Metabasalts as sources of metals in orogenic gold deposits. Miner. Deposita 50 (3), 373–390.

Popov, G.G., Popov, B.G., Miziryak, D.G., 2017a. The Kedrovskoe gold ore field (geologic structure and ore potential). Regional'naya Geologiya i Metallogeniya 69 (1), 80–87.

Popov, G.G., Popov, B.G., Muratshin, Kh.Kh., Miziryak, D.G., 2017b. Petrochemical characteristics of igneous rocks and hydrothermal-metasomatic deposits of the Kedrovskoe gold ore field. Razvedka i Okhrana Nedr, No. 9, 27–32.

Qian, Z., 1987. Trace elements in galena and sphalerite and their geochemical significance in distinguishing the genetic types of Pb–Zn ore deposits. Chinese J. Geochem. 6 (2), 177–190.

Reeson, K.J., Stanley, C.J., Jeynes, C., Grime, G., Watt, F., 1990. PIXE analysis to determine the trace-element concentrations in a series of galena (PbS) specimens from different localities. Nucl. Instrum. Methods Phys. Res., Sect. B 45 (1–4), 327–332.

Renock, D., Becker, U., 2011. A first principles study of coupled substitution in galena. Ore Geol. Rev. 42 (1), 71–83.

Ridley, J.R., Mikucki, E.J., Groves, D.I., 1996. Archean lode-gold deposits: fluid flow and chemical evolution in vertically extensive hydrothermal systems. Ore Geol. Rev. 10, 279–293.

Rytsk, E.Yu., Amelin, Yu.V., Rizvanova, N.G., Krimsky, R.Sh., Mitrofanov, G.L., Mitrofanova, N.N., Perelyaev, V.I., Shalaev, V.S., 2001. Age of rocks in the Baikal–Muya Foldbelt. Stratigr. Geol. Correl. 9 (4), 315–326.

Rytsk, E.Yu., Kovach, V.P., Yarmolyuk, V.V., Kovalenko, V.I., Bogomolov, E.S., Kotov, A.B., 2011. Isotopic structure and evolution of the continental crust in the East Transbaikalian segment of the Central Asian Foldbelt. Geotectonics 45 (5), 349–377.

Safina, N.P., Obukhov, A.A., Blinov, I.A., 2015. Tin and silver minerals from the Nikolaevskoe gold deposit (Yenisei Ridge, Krasnoyarsk Krai, Russia). Mineralogy, No. 2, 3–8.

Skuzovatov, S.Yu., Sklyarov, E.V., Shatsky, V.S., Wang, K.-L., Kulikova, K.V., Zarubina, O.V., 2016. Granulites of the South Muya block (Baikal–Muya Foldbelt): Age of metamorphism and nature of protolith. Russian Geology and Geophysics (Geologiya i Geofizika) 57 (3), 451–463 (575–591).

Standish, C.D., Dhuime, B., Chapman, R.J., Hawkesworth, C.J., Pike, A.W.G., 2014. The genesis of gold mineralisation hosted by orogenic belts: A lead isotope investigation of Irish gold deposits. Chem. Geol. 378–379, 40–51.

State Geological Map of the Russian Federation. Scale 1 : 1,000,000 (Third Generation). Aldan–Transbaikalia Series. Sheet N-50: Sretensk. Explanatory Note [in Russian], 2010. Kartograficheskaya Fabrika VSEGEI, St. Petersburg.

Tsygankov, A.A., Vrublevskaya, T.T., Konnikov, E.G., Posokhov, V.F., 1998. Geochemistry and petrogenesis of granitoids of the Muya Complex (East Siberia). Geologiya i Geofizika (Russian Geology and Geophysics) 39 (3), 361–374 (371–385).

Tsygankov, A.A., Litvinovsky, B.A., Jahn, B.M., Reichow, M.K., Liu, D.Y., Larionov, A.N., Presnyakov, S.L., Lepekhina, Ye.N., Sergeev, S.A., 2010. Sequence of magmatic events in the Late Paleozoic of Transbaikalia, Russia (U–Pb isotope data). Russian Geology and Geophysics (Geologiya i Geofizika) 51 (9), 972–994 (1249–1276).

Vanin, V.A., Tatarinov, A.V., Gladkochub, D.P., Mazukabzov, A.M., Molochnyi, V.G., 2017. The role of dynamometamorphism in the formation of the Mukodek gold field (North Pribaikalie). Geodynamics & Tectonophysics 8 (3), 643–653.

Vaughan, D.J., Craig, J.R., 1978. Mineral Chemistry of Metal Sulfides. Cambridge University Press, Cambridge.

Weir, Jr., R.H., Kerrick, D.M., 1987. Mineralogic, fluid inclusion, and stable isotope studies of several gold mines in the Mother Lode, Tuolumne and Mariposa counties, California. Econ. Geol. 82, 328–344.

Wen, H., Zhu, C., Zhang, Y., Cloquet, C., Fan, H., Fu, S., 2016. Zn/Cd ratios and cadmium isotope evidence for the classification of lead–zinc deposits. Sci. Rep. 6 (25273).

Yarmolyuk, V.V., Kovach, V.P., Kozakov, I.K., Kozlovsky, A.M., Kotov, A.B., Rytsk, E.Yu., 2012. Mechanisms of continental crust formation in the Central Asian Foldbelt. Geotectonics 46 (4), 251–272.

Zapadnaya Gold Mining Limited, 2018. http://www.zapadnaya.ru/qa/Kedrovskoe.html [in Russian], http://www.zapadnaya.com/qa/Kedrovskoe.html [in English].

Zhmodik, S.M., Postnikov, A.A., Buslov, M.M., Mironov, A.G., 2006. Geodynamics of the Sayan–Baikal–Muya accretion–collision belt in the Neoproterozoic–Early Paleozoic and regularities of the formation and localization of precious-metal mineralization. Russian Geology and Geophysics (Geologiya i Geofizika) 47 (1), 187–200 (183–197).

Zlobina, T.M., Murashov, K.Yu., Kotov, A.A., 2014. Modeling of the structural-dynamic conditions of gold-quartz vein localization in the Irokinda deposit (Muyskiy gold region). Geology and Mineral Resources of Siberia, No. 3, Part 2, 62–68.

Editorial responsibility: A.S. Borisenko